AN ABSTRACT OF THE THESIS OF

Nathan A.Barnett for the degree of Master of Science in Nuclear Engineering
Presented on July 25, 2008.

Title: Binary Stochastic Media Transport: A Coupled Mesh Based Method

Abstract approved:

_____

Todd S. Palmer

Transport in a binary stochastic media has been an area of interest for many applications over the past three decades. Many different methods have been attempted, most based on the Levermore-Pomraning coupled transport model. However, this method has never been able to correctly solve problems where a large amount of scattering is present. Many modifications of the code involve making assumptions that simplify a term in the balance equation that involves material transition probabilities inside of a cell.

We introduce a new method, where all transport is carried out on a mesh. Using the mesh, the difficult coupling term is not present in the balance equation.

We explore how the new coupled equations perform in a variety of problems. Though not all facets of the equations are investigated (e.g. interior source problems), the equations perform very well. Results are achieved with relative errors under 1% where past methods produced errors of at least 30% and up to 77% in similar cases.

Binary Stochastic Media Transport: A Coupled Mesh Based Method

by

Nathan A. Barnett

A THESIS

Submitted to

Oregon State University

in partial fulfillment of
the requirements for the
degree of

Master of Science

Presented July 25, 2008
Commencement June 2009

Master of Science thesis of Nathan A. Barnett presented on July 25, 2008.

APPROVED:

Major Professor, representing Nuclear Engineering

Head of the Department of Nuclear Engineering and Radiation Health Physics

---

Dean of the Graduate School

I understand that my thesis will become part of the permanent collection of Oregon State University libraries. My signature below authorizes release of my thesis to any reader upon request.

Nathan A. Barnett, Author

ACKNOWLEDGEMENTS

Thanks to my parents for listening when I needed it, sending me random notes and gifts, and putting up with my antics for longer than anyone should have to do so.

Thanks to my grandparents for pushing me to finish school, providing generous help whenever it was needed, and for setting an example for me to follow.

Special thanks go to my SOLP, Julie, for taking care of me when I was too busy to do so myself.

Matt “England” Cleveland – I couldn’t have made it without your help: double-checking my work, listening to hours of complaints, and toiling together in the darkness of the fish-bowl into the depths of the night.

Wes Frey – you kept me straight and focused on the goal (not the beer goal, the degree one… well, maybe the beer goal, too).

I would like to sincerely thank Todd Palmer for guiding me in producing quality work, for answering late-night emails and weekend phone calls.

TABLE OF CONTENTS

Page

LIST OF FIGURES

LIST OF FIGURES (Continued)

LIST OF FIGURES (Continued)

Figure Page

LIST OF TABLES

Binary Stochastic Media Transport: A Coupled Mesh Based Method

1 Introduction

The Boltzmann equation for neutral particle transport can be a very challenging equation to solve. It is an integro-differential equation whose solution can be a very complex function of any of its seven independent variables (three space, two angle, energy, time). While some problems can be solved analytically, most problems must be simplified in order to write a set of equations that can be solved by a computer. These simplifications directly relate to the phase space of the Boltzmann equation and are chosen for each application: a reactor physicist may assume the problem of interest is time independent, a shielding problem may reduce the equation to only one energy group or the treatment of a cancer patient may require very few discrete angles. Whether for astrophysics, thermal radiative transfer, electro-magnetic analysis, or plasma physics several classes of methods exist for solving the simplified Boltzmann equation.

Monte Carlo methods use pseudorandom numbers, picking many points to approximate integrals. Many points must be chosen in order to calculate accurate mean quantities with acceptable statistical error, an often time consuming task. Application of this integration method to neutral particle transport can make the method seem very physical. Often referred to as a random walk, a particle is started in the problem and, based on probabilities, is moved through scattering events and geometric regions until it is absorbed or leaves the problem. After repeating many times and tallying the distance each particle travels through a region of interest, the solution to the problem is reached with some statistical error. While this is a very common way of calculating the flux, other methods do exist, including absorption estimators and collision estimators [**1**]. MCNP (Monte Carlo N-Particle) is a code developed at Los Alamos National Labs that uses this method and is thought of as the gold standard in particle transport in many fields. It has been used to “find water on Mars and aided doctors battling cancer on Earth”, design nuclear reactors and even radiation detectors [**2**].

Deterministic methods involve no randomness and will always provide the exact same answer, given the same starting information. Although these methods are not as intuitive as the Monte Carlo method, they can be very fast and provide answers at every point in the problem. Like Monte Carlo methods, the precision of the answer improves with run-time. Unlike Monte Carlo methods, deterministic methods produce error through computer-based math, not statistical error [**1**].

Hybrid methods also exist that try to capitalize on the benefits of both the Monte Carlo and deterministic methods. These methods have not been widely used up to this point, but much work is currently underway to explore their behavior in a wide variety of physical problems [**3, 4, 5**].

Deciding which method to use with which data sets and geometry to solve a given problem is an art. Some discretization techniques may involve a large number of degrees of freedom, requiring excessive computational time for the accuracy required. Other methods may not capture the important portions of a solution or yield answers with too much numerical error.

In general, the problem geometry is divided into regions with uniform material properties. With a Monte Carlo radiation transport program such as MCNP areas of interest are identified where the variance in the solution must be small, and larger variances are acceptable in the remaining regions.

With a deterministic method, energy, space, particle direction, and time are discretized with resolution that will generate solutions with sufficiently small numerical error. A transport equation is developed for each of the regions, with data specific to that region and the equations must be solved simultaneously.

A special situation arises when the materials (and the associated nuclear cross sections) are known, but the locations of those materials are known only

probabilistically. Such is the case in atmospheric transport, where solar radiation is modeled traveling through a cloud (water and air, but randomly placed) [**6**]. The human lung, too, can be categorized in this way, as lung tissue and air randomly distributed in space [**7**]. In addition to atmospheric sciences and medical physics, problems of interest have also arisen in astrophysics and criticality work, as well as applied mathematics [**8, 9, 10**]. These problems can be divided up into spatial regions, but the data to use for each of the regions is stochastic. In this case, it becomes impossible to write an exact set of equations to describe the problem.

One approach to generate numerical solutions to the Boltzmann equation in this situation is to sample a realization from the statistical material distribution functions, and solve the transport equation for this realization. The process is repeated many times and the results are averaged. The ensemble average flux and the associated variance allow solution confidence intervals to be computed. Many realizations may be necessary to obtain small variances. This method is often referred to as the "brute force" method [**7**].

Another approach involves ensemble averaging the analytic transport equations "up front" and developing numerical techniques for the solution of these material averaged equations. The material averaged equations can be manipulated to produce approximate ensemble average fluxes. This method was initially developed by Levermore and Pomraning [**11**]. Their method involves coupled equations for the conditional average flux in each material.

One limitation of this approach is the necessity to use an approximate closure relationship. This involves relating the material interface averaged fluxes to the material averaged fluxes [**12**]. The original closure approximation is only exact for a Markovian transport process [**13**].

For this reason, the majority of the research on stochastic mixture transport has dealt exclusively with an exponential distribution of material "chunk" sizes,

measured using a chord length distribution [**12, 11, 14**]. These exponential chord length distributions are consistent with Markovian mixing statistics, which improve the validity of the LP equations.

However, as soon as scattering is added, there is no longer a Markovian transport process and the method can produce solutions with very large errors when compared to benchmark solutions generated using the brute force method [**15**]. This has left these equations with a very limited scope of usability.

While attempts have been made to develop improved closures or to adjust material cross-section data to provide better answers, approximate models for coupled stochastic mixture transport still suffer from unacceptably large errors, particularly for problems with highly scattering regions. [**16**].

By applying several simplifications in the discretization of the transport equation, it is possible to derive coupled ensemble averaged transport equations without the difficult closure term and without a loss of physicality. The resulting equations require only that the distribution of materials within the problem are known.

If the problem of interest is always solved on a mesh, where the mesh lies in exactly the same place for each realization, then the material interface locations are always known. Then, if the mesh can be filled with two materials in a controlled yet random manner, the average distribution of materials can accurately be characterized.

With a known statistical distribution of materials, the coupled equations can be solved without the difficulties of former closures, yielding accurate solutions in both the Markovian case and otherwise.

In this thesis we address the following research questions:

1) Can exponential chord length distributions be modeled using realizations with the same orthogonal spatial mesh? This may show that we may use this in place of 3D attempts with spheres in the past and achieve similar results. Furthermore, we would be able to achieve exact results when in a purely absorbing medium.
2) Can we derive coupled stochastic mixture transport equations that do not require a closure term relating interface-average and material-average quantities?
3) Can we calculate the coupling probabilities for the equations and achieve the correct results? This could be easy and cheap data to calculate as a pre-processing step in solving the coupled equations.
4) How do the results from the new mesh-based coupled binary stochastic mixture transport equations compare to the results from other models and to benchmark results from the brute force method?

Our goal is to develop a new coupled transport methodology that will provide fast and accurate solutions to problems involving stochastic media.

2 Literature Review

In the 1980s Levermore and Pomraning investigated the scenario of solving a problem with stochastically placed material [**11**]. By simplifying the problem to one with only two materials and assuming a Markovian distribution of the materials, they were able to formulate coupled transport equations that described the average flux in each material. However, the equations proved too difficult to derive in 2D and 3D when scattering was involved.

Vanderhaegen showed that, in the case of non-scattering, Markovian distributions, the transport process is Markovian. He then explained that, in fact, the LP equations are exact with any Markovian process, as Levermore and Pomraning had seen. He then introduced the idea of using the Liouville master equation instead (which is exact in the Markovian case, as well) in hopes that it could better handle scattering [**13**].

Later, Adams, Larsen and Pomraning expanded upon these equations, showing that they could be used with any distribution of materials, as long as the distribution was known. More importantly, the closure term was modified to help with scattering. The interface average term from the master equations was replaced by a problem interior average, approximated using an upwind scheme. They benchmarked the equations in 1D rod and slab geometries, looking only at the transmitted and reflected angular fluxes at each end of the problem [**12**].

In hopes of increased computational speed, Graziani compared several other transport codes using problems where the LP equations would accel. The paper used the results of numerical test problems to empirically modify the cross sections in order to achieve good results. In addition, the material allocation algorithm used was designed to simulate cracks and approach a Cauchy or Poisson distribution [**17**].

Olson, in 2006, showed that the LP equations produce poor answers in 2D and 3D when scattering is introduced because of problems with the closure term which requires a Markovian transport process. He showed that in 2D and 3D, with a distribution of impenetrable spheres, an exponential distribution of materials could not be achieved and therefore a Markovian transport process could not be achieved either. Like Graziani, he modified the cross sections to improve how the equations handle scattering [**18, 14**].

Research has also expanded into renewal theory [**19, 20, 21, 22, 23, 24**], asymptotic limits [**25, 26, 8**], eigenvalue problems [**27, 28**], anisotropic scattering treatments [**29, 30, 31**], and multiple attempts at different closures with limited success [**32, 33, 34**].

3 Methods

In choosing to discretize the coupled transport equations on a mesh, it is hoped that the difficult closure term seen in past research will not be required. The resulting coupled binary stochastic mixture transport equations should yield accurate solutions in purely absorbing problems, as before, and in problems with significantly scattering materials.

In order to test the validity of the new coupled equations, the “brute force” method of averaging the standard transport solution over many realizations will be taken as the benchmark results. The benchmark solution, calculated through a post-transport average can be compared to the new coupled method, where ensemble averaged solutions are averaged up-front.

With the brute force method, many realizations of the stochastically filled mesh must be produced and the transport solutions to these realizations averaged. The coupled BSM transport methods do not require the generation of realizations because they involve quantities which are averaged over the mixing statistics. However, both the LP method and the new coupled method proposed in this thesis require a characterization of the mesh: for the LP equations, a parameter from a chord length distribution is needed and for the new coupled method a cell transition probability will be needed. Both of these can be considered as pre-processing steps and can be calculated from problem realizations. Therefore, the algorithm used to generate realizations is an important aspect of all three approaches to the BSM problem.

In this section of the thesis, how the mesh is filled and verified will first be discussed. Next, the characterization of the material distribution within a mesh will be discussed. A chord length distribution will be explained, followed by a cell transition probability. Then, the transport equation will be discretized using a diamond differencing scheme and the solution of the “brute force” method will be

discussed. Finally, the same diamond differencing scheme will be used in the development of the new coupled method.

3.1 Filling the Mesh

As discussed earlier, previous successful work in the area of stochastic transport has dealt almost entirely with an absorbing material in a Markovian, or exponential, distribution.

Adams et. al have shown that, although distributions other than Markovian have been considered, the best results from the LP equations have been obtained from a Markovian distribution of material [**12, 17, 24**].

Olson et. al attempted to extend the 1D Markovian distributions used in previous work and to 2D and 3D; spheres of absorbing material were randomly placed in a background medium. It was shown that randomly sized spheres of absorbing material, mixed as 10% of the total problem volume, and placed randomly in an infinite medium would produce a Markovian distribution in the background material [**14**].

Using an orthogonal mesh, the randomly placed spheres can be mimicked by filling random cells until the mesh reaches the correct volume fill percentage (10% in this case, although any amount could be used). Then, using a large number of chords, a CLD can be calculated and compared to the desired Markovian distribution. Once again, this problem configuration is not necessary, but it is a good starting point from which to continue, based on previous work.

In order to properly fill the mesh the following steps are followed:

1. Fill each cell in the mesh with the background material (material 1).
2. Determine the number of cells to fill with material 0 based on the desired fill percentage:
3. Randomly choose three integers: an x, y and z cell location.

4. Repeat step 3 until the appropriate number of cells are filled.

This unbiased random process ensures that, in the limit of a large number of realizations, each cell will contain the two materials in their respective fill percentages. Verifying that the mesh is being filled in this manner ensures that the random number generator is working properly and it can also provide an idea of how many realizations are needed to achieve a satisfactory statistical sampling of meshes. To verify that the mesh is being filled evenly over a large number of realizations the following calculation can be performed:

1. Fill the mesh for a given realization.
2. Walk through the mesh once, and tally in each cell if it is filled by material 0.
3. Repeat the above steps many times without resetting the tally in each cell.

If the mesh is being filled uniformly and randomly over the number of realizations, then the tally in each cell should approach the same number.

3.2 Mesh Characterization

Many different types of distributions can occur in a statistical mixture. One way of describing how the materials are dispersed, is by a chord length distribution (CLD). A CLD, $p_n(x)\,dx$, is the probability that the chord length in material n lies between x and x+dx.

As mentioned earlier, a Markovian CLD is often used in stochastic transport problems and takes the form

$$p(x) = \frac{1}{\lambda} e^{-\lambda x} \qquad \text{Eq. 1}$$
$$where\ \lambda = mean\ chord\ length$$

For this distribution of materials, the analytical transport solution is known when the problem is time independent and purely absorbing. It therefore provides a basis for comparison to the numerical answers. The LP equations utilize the chord length distribution, employing λ as a coupling parameter.

A CLD can be calculated by taking a given realization on a mesh, starting at a random location on a random side, and tracing a straight line in a random direction until the other side of the problem is reached. The chord lengths in each of the materials can then be binned. After an appropriately large number of chord lengths have been calculated, the resulting tally bins can be plotted and a curve can be fit. An example of a set of chords within a mesh is shown in figure 1**.**

The algorithm for calculating a single chord in a mesh filled with two materials is as follows:

1. Each of the six sides of the mesh is given an integer identifier, numbered one through six. Randomly select a side of the mesh.
2. Randomly select a location on this plane within and including the problem boundaries.
3. Steps 1 and 2 produce a starting point for the chord. Repeat these steps to find an end point on any other side of the problem.
4. Based on the direction of travel and beginning with the starting point, calculate the distance to the next three (3) planes that the chord will intersect by fixing the x, y, or z coordinate and solving for the other two.
5. Use the shortest distance to select the next point on the chord and move the current position of the chord to that location.
6. If the material in the next cell is different than the one that was just passed though, add one to a tally for distance just traveled by the chord. Each tally is referred to as a bin – a chosen range of chord lengths where the first bin counts lengths of 0 to dS and the last bin counts lengths of S-dS to S and S is the maximum length that a chord can achieve.
7. If the material in the next cell is the same, continue calculating the length of the current chord by adding the next calculated distance to the one just calculated.
8. Repeat, cell by cell, until the boundary of the mesh is reached.

In order to produce a distribution, many chords are calculated and binned. These binned results are graphed and a trend line can be fit.

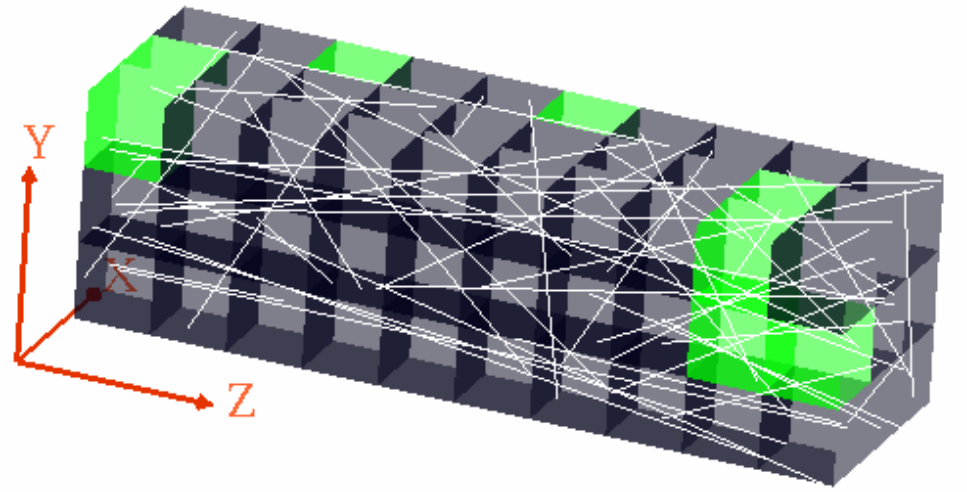

Figure 1 – Calculating a CLD

Another method of characterizing the distribution of materials in a mesh is with a cell transition probability (CTP). There exists on each interior face of the orthogonal mesh a set of probabilities of material transition on that surface. With a distribution of two materials, as is explored in this thesis, four probabilities exist for each surface of a given interior cell: the given cell contains material 0 and material 1 lies on the other side, the given cell contains material 0 and material 0 lies on the other side, the given cell contains material 1 and material 1 lies on the other side, and the given cell contains material 1 and material 0 lies on the other side.

Given that the mesh is being filled homogeneously in space, each cell should have the same probability of being filled with material 0 (or material 1). It follows that every surface, then, should have the same set of probabilities given a very large number of realizations.

Many other types of material distributions may have differing CTPs from cell to cell. The data from these CTPs can still be used in the same manner to solve the coupled equations developed later.

Calculating the CTP can be accomplished using the following algorithm:

1. Create a realization of the mesh.
2. March through the interior cells of the mesh, tallying which transitions occur on each of the cell faces.
3. Repeat this process until an acceptably low statistical variance is achieved.
4. Normalize the results.

Given that the problem is being filled correctly and enough mesh realizations tallied, the set of probabilities in each cell should be statistically identical.

3.3 Benchmarking

Both the "brute force" method and the new coupled method solve the transport equation in a very similar manner. The 3D codes that will be used are based on a diamond differencing scheme and uses a standard transport sweep.

In a standard transport sweep, an incident angular flux is assumed known on one side of a cell. By assuming the corresponding cell-averaged angular flux is the average of the two cell sides, the transport equation can be rearranged to solve for the cell-averaged quantity and the angular flux on the opposite side of the cell. This flux is then used as the known incident flux on the next cell. In this manner, the spatial mesh is swept from one corner to another, in the direction of particle flow. After a full sweep, the cell-averaged scalar flux in each cell is calculated as a weighted sum of the cell-averaged angular fluxes. The scattering term on the right hand side of the equation, which contains the cell-averaged scalar flux, is updated. Because the equations have changed, due to the update in the scattering term, this process is repeated, until the scalar flux reaches convergence.

$$\varepsilon > \left|\Phi_i^{l+1} - \Phi_i^{l}\right| \qquad \text{Eq. 2}$$

where l denotes the number of the sweep $\cdot$
and ε is a predetermined value

Diamond differencing is a simple scheme that must be used with care to avoid destabilizing the transport answer. When cells become optically thick, diamond difference method can generate negative angular fluxes and unphysical oscillating solutions. Care must be taken in choosing cell widths to avoid this problem. Optical thickness is calculated using equation (3).

$$\tau = \frac{\sigma_a \cdot dx}{\mu}$$

where dx is the width of the cell
and μ *is the angle of particle travel*

Eq. 3

We begin with the transport equation, which is simply a balance equation stating that the change in flux is due to the influx and outflux.

$$\frac{1}{\nu}\frac{\partial \psi\left(\vec{r}, E, \hat{\Omega}, t\right)}{\partial t} + \hat{\Omega} \cdot \nabla \psi\left(\vec{r}, E, \hat{\Omega}, t\right) + \sigma_t \psi\left(\vec{r}, E, \hat{\Omega}, t\right) = \int_{4\pi} d\hat{\Omega}' \int_0^{\infty} dE' \sigma_s\left(E' \to E, \hat{\Omega}' \to \hat{\Omega}\right) \psi\left(\vec{r}, E', \hat{\Omega}', t\right) + S\left(\vec{r}, E, \hat{\Omega}, t\right)$$

Eq. 4

Now we assume that the equation is time independent (steady state).

$$\hat{\Omega} \cdot \nabla \psi\left(\vec{r}, E, \hat{\Omega}\right) + \sigma_t \psi\left(\vec{r}, E, \hat{\Omega}\right) = \int_{4\pi} d\hat{\Omega}' \int_0^{\infty} dE' \sigma_s\left(E' \to E, \hat{\Omega}' \to \Omega\right) \psi\left(\vec{r}, E', \hat{\Omega}'\right) + S\left(\vec{r}, E, \hat{\Omega}\right)$$

Eq. 5

Next, we consider isotropic scattering, which simplifies the right hand side of equation (5). We also normalize the scattering term to 4π.

$$\hat{\Omega} \cdot \nabla \psi\left(\vec{r}, E, \hat{\Omega}\right) + \sigma_t \psi\left(\vec{r}, E, \hat{\Omega}\right) = \int_{4\pi} d\hat{\Omega}' \int_0^{\infty} dE' \frac{\sigma_s(E' \to E)}{4\pi} \psi\left(\vec{r}, E', \hat{\Omega}'\right) + S\left(\vec{r}\right)$$

Eq. 6

If we integrate this equation over all energy

$$\hat{\Omega} \cdot \nabla \psi\left(\vec{r},\hat{\Omega}\right) + \sigma_t \psi\left(\vec{r},\hat{\Omega}\right) = \frac{\sigma_s}{4\pi} \int_{4\pi} d\hat{\Omega}' \psi\left(\vec{r},\hat{\Omega}'\right) + S\left(\vec{r}\right) \qquad \text{Eq. 7}$$

Performing the integral over angle on the right hand side of equation (7) yields

$$\hat{\Omega} \cdot \nabla \psi\left(\vec{r},\hat{\Omega}\right) + \sigma_t \psi\left(\vec{r},\hat{\Omega}\right) = \frac{\sigma_s}{4\pi} \Phi\left(\vec{r}\right) + S\left(\vec{r}\right) \qquad \text{Eq. 8}$$

We will now develop the discretized version of this equation by introducing ideas in one dimension and, later, extending these ideas into three dimensions.

The direction variable is discretized by dividing angular space into a set number of angles. A discretized angular variable is denoted with the *m* subscript. Note that in 1D, integration of the scattering term only cancels out part of the normalization factor.

$$\mu_m \frac{\partial \psi_m}{\partial x} + \sigma_t \psi_m(x,\mu) = \frac{\sigma_s}{2} \Phi(x) + S(x) \qquad \text{Eq. 9}$$

Each spatial cell as a homogeneous region with two edges over which our simplified balance equation holds true. Diamond differencing assumes that the cell-average angular flux is the simple mean of the fluxes on either edge of the cell. Cell-averaged quantities are denoted with the subscript i, i+1, etc. and cell-edge quantities have subscripts of i+1/2 or i-1/2.

$$\mu_m \frac{\partial \psi_{m,i}}{\partial x} + \sigma_{t_i} \psi_{m,i} = \frac{\sigma_{s_i}}{2} \Phi_i + S_i \qquad \text{Eq. 10}$$

where

$$\psi_{m,i} = \frac{1}{2}\left(\psi_{m,i-\frac{1}{2}} + \psi_{m,i+\frac{1}{2}}\right) \qquad \text{Eq. 11}$$

We integrate equation (10) over a cell.

$$\frac{\mu_m}{\Delta x}\left(\psi_{m,i+\frac{1}{2}} - \psi_{m,i-\frac{1}{2}}\right) + \sigma_{t_i} \psi_{m,i} = \frac{\sigma_{s_i}}{2} \Phi_i + S_i$$

and Eq. 12, 13

$$\Phi_i = \sum_{m=0}^{N} \left(w_m \psi_{m,i}\right)$$

To solve this equation, the angular flux on the incident edge is known from boundary conditions or from a previous cell calculation and the cell-averaged scalar flux is known from an initial guess or a previous iteration.

$$\frac{\mu_m}{\Delta x_i}\left(2\psi_{m,i} - \psi_{m,i-\frac{1}{2}} - \psi_{m,i-\frac{1}{2}}\right) + \sigma_{t_i}\psi_{m,i} = \frac{\sigma_{s_i}}{2}\Phi_i + S_i$$

$$\therefore \psi_{m,i} = \left(\psi_{m,i-\frac{1}{2}} + \frac{\Delta x_i}{2\mu_m}\right)\frac{\frac{\sigma_{s_i}}{2}\Phi_i + S_i}{1 + \sigma_{t_i}\frac{\Delta x_i}{2\mu_m}} \quad , \ \mu_m > 0 \qquad \text{Eq. 14, 15}$$

and

$$\psi_{m,i+\frac{1}{2}} = 2\psi_{m,i} - \psi_{m,i-\frac{1}{2}}$$

In this manner, if the incident angular flux on one side is known, the corresponding flux at the other side and the cell-average can be computed.

Equations (14) and (15) hold in each spatial cell of the mesh, for each direction in the quadrature set. After solving for both edge fluxes and the cell averaged flux in the first cell, the fluxes in the next cell can be solved by setting the corresponding angular fluxes that lie on the surface between the cells equal.

$$\psi_{m,i+\frac{1}{2}} = \psi_{m,(i+1)-\frac{1}{2}} \qquad \text{Eq. 16}$$

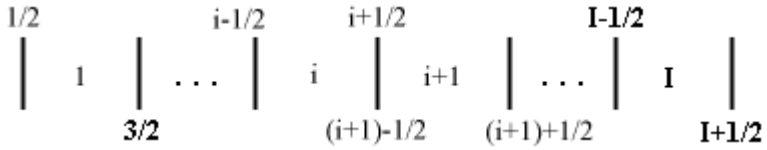

Figure 2 – 1D Cell Labeling

When the cells have been swept in the positive directions and the boundary has been reached, the mesh is swept in the negative directions. Notice that the equation used in the forward sweep must be changed slightly for the backward sweep.

$$\psi_{m,i} = \left(\psi_{m,i+\frac{1}{2}} - \frac{\Delta x_i}{2\mu_m}\right)\frac{\frac{\sigma_{s_i}}{2}\Phi_i + S_i}{1 - \sigma_{t_i}\frac{\Delta x_i}{2\mu_m}} \quad , \ \mu_m < 0 \qquad \text{Eq. 17, 18}$$

and

$$\psi_{m,i-\frac{1}{2}} = 2\psi_{m,i} - \psi_{m,i+\frac{1}{2}}$$

Common boundary conditions include vacuum and reflecting boundaries. On a reflecting boundary, the incident angular flux is set equal to the outgoing flux.

Once all sweeps have been completed, then the new scalar flux can be calculated as a weighted sum of the cell averaged angular fluxes.

However, the flux term on the right side really has an angular flux in it and up until now we assumed we knew it. Since we know all the angular fluxes now, we can calculate Φ in each cell by summing the weighted angular fluxes in that cell.

After each sweep of the mesh, we must recalculate Φ. We can determine if the solution has been reached by testing convergence. This is done by looking at the difference between successive flux iterates (Equation 2). This is often called source iteration and provides a very physical method for estimating the speed of convergence. If particles, on average, make few collisions before being removed by, absorption, leakage, or scattering out of the energy group convergence will be rapid [**1**].

There are times when simply sweeping the mesh repeatedly will not work. If the cell width is very large and the total cross section is large, then the cell is said to be optically thick. If too many neutrons are attenuated in a given cell, then negative, unphysical fluxes can be generated. For diamond difference, the optical thickness (τ) must remain less than two ($\tau<2$) and can be calculated using equation (3). This limit can be derived by examining the error incurred by the diamond difference method.

In the purely absorbing case the exact solution in known across a cell

$$\psi_{i+\frac{1}{2},m} = \psi_{i-\frac{1}{2},m} e^{-2\cdot h} \qquad \text{Eq. 19}$$

The solution to the diamond difference method is also known

$$\psi_{i+\frac{1}{2},m} = \psi_{i-\frac{1}{2},m} \left(\frac{1-h}{1+h}\right) \qquad \text{Eq. 20}$$

where, in equation () and in equation ()

$$h = \frac{\sigma_t \cdot \Delta x}{2 \cdot |\mu|} \qquad \text{Eq. 21}$$

By subtracting equation (20) from equation (19), the error incurred in each cell by diamond difference can be calculated. In a mesh with equal cell sizes, the error is compounded by each cell and grows linearly throughout the problem.

Now that we have the 1D case, it is very easy to expand to 3D. The only things that change are the integration of the scattering term and the streaming term. We will label the cell surface angular fluxes with a superscript denoting the coordinate to which the surface is parallel.

$$\begin{aligned} &\bigtriangledown \psi_{m,i} + \sigma_{t_i} \psi_{m,i} = \frac{\sigma_{s_i}}{4\pi} \Phi_i + S_i \\ &\Rightarrow \psi_{m,i} = \frac{\frac{2\mu_m}{\Delta x_i} \psi^x_{m,i-\frac{1}{2}} + \frac{2\eta_m}{\Delta y_i} \psi^y_{m,i-\frac{1}{2}} + \frac{2\xi_m}{\Delta z_i} \psi^z_{m,i-\frac{1}{2}} + \frac{\sigma_s}{4\pi} \Phi_i + S_i}{\frac{2\mu_m}{\Delta x_i} + \frac{2\eta_m}{\Delta y_i} + \frac{2\xi_m}{\Delta z_i}} \end{aligned} \qquad \text{Eq. 22}$$

The angular fluxes are calculated across the cell just as they were in the 1D case.

$$\begin{aligned} \psi^x_{m,i+\frac{1}{2}} &= 2\psi_{m,i} - \psi^x_{m,i-\frac{1}{2}} \\ \psi^y_{m,i+\frac{1}{2}} &= 2\psi_{m,i} - \psi^y_{m,i-\frac{1}{2}} \\ \psi^z_{m,i+\frac{1}{2}} &= 2\psi_{m,i} - \psi^z_{m,i-\frac{1}{2}} \end{aligned} \qquad \text{Eq. 23}$$

It is important now to describe the order in which the 3D problem is swept and the angles that we must use.

In order to integrate angular flux, we must choose how the angles are discretized. In 1D a scheme such as Simpson's rule can be used. However, when working in higher dimensions these schemes become impossible to use. One method of integration that is similar, but can be used in higher dimensions is a Gauss quadrature.

In a Gauss-Legendre quadrature, angles and weights are chosen such that the Legendre polynomials of order 2N-1 are integrated exactly. Many other similar methods exist, each with a specific advantage. However, the scattering term is typically described using Gauss-Legendre polynomials and greater efficiency can

be achieved in the solution of the problem if both the scattering term and fluxes are defined in the same manner.

This method of angular discretization is often called the S_N or discrete ordinates method, where *N* is the number of angles being used. The GL quadrature sets are usually symmetric and *N* is usually an even number. The S_4 quadrature set in 1D, for example, discretizes the direction variable (μ) into four angles: two positive and two negative. In 3D, S_4 quadrature results in 24 (N(N+2)) total angles or ordinates. The extra accuracy gained through the use of higher order quadratures introduces more angles and computational cost quite rapidly (S_6=48, S_{10}=120, etc.).

Each octant of ordinates is "swept" separately in the direction of particle flow. For example, in the first octant, angles in all three directions are positive. A sweep can therefore begin at the origin and those angular fluxes for that octant of ordinates be solved through to the opposite corner of the mesh. In the second octant, ξ and η are positive, but μ is negative. A sweep of the mesh can begin where y and z are at their minimum and x is at its maximum. The sweep can be solved in the positive y and z directions and in the negative x direction.

Eight sets of sweeps, one for each octant, must be completed during the transport calculation. As in the 1D case, the scalar flux can then be updated.

3.4 Coupled Equations

The derivation of coupled equations is an easy extension of the derivation of the standard S_N code. We follow the derivation of the LP equations and show where the mesh based BSM method differs. We derive these equations in 1D, but using the analogous derivation from above it is easy to extend to 3D.

This derivation assumes there are two materials in the stochastic mixture. We also assume that material cross sections and mixing statistics are known. We define the characteristic function χ, such that

$$\chi_i^n = \begin{cases} 1, \textit{ if cell i is filled by material n} \\ 0, \textit{ otherwise} \end{cases} \qquad \text{Eq. 24}$$

We now multiply the standard balance equation by χ. However, to obtain true balance for the volume, a term must be added to the end that accounts for particle loss and addition due to flow across internal surfaces Γ. The dependence on r and t are still applicable, but removed for readability.

$$\begin{aligned} &\frac{1}{\nu}\frac{1}{\partial t}\int_V \chi_i\, \psi\,(\Omega)\, dr = \\ &\quad \int_V \chi_i\, S_i\,(\Omega)\, dr - \int_V \chi_i\, \sigma_i\, \psi\,(\Omega)\, dr + \frac{1}{4\pi}\int_V \chi_i\, \sigma_{s_i}\, dr \int_{4\pi} \psi\,(\Omega')\, d\Omega' \\ &\quad - \int_B \chi_i\,(n\cdot\Omega)\, \psi\,(\Omega)\, ds - \int_\Gamma (n\cdot\Omega)\, \psi\,(\Omega)\, ds \end{aligned} \qquad \text{Eq. 25}$$

In order to ensemble average this equation over all realizations, we define

$$p_i\,(r,t) = \left\langle \chi_i\,(r,t) \right\rangle,$$

$$\psi_i\left(r,\Omega,t\right) = \frac{\left\langle \chi_i\,(r,t)\, \psi\left(r,\Omega,t\right)\right\rangle}{\left\langle \chi_i\,(r,t)\right\rangle} \qquad \text{Eq. 26, 27}$$

where the $\langle\cdot\rangle$ notation means ensemble average.

By taking this into account, an ensemble average of equation ()

$$\begin{aligned} &\frac{1}{\nu}\frac{1}{\partial t}\int_V p_i\, \psi_i\,(\Omega)\, dr + \int_\nu (n\cdot\Omega)\, p_i\, \psi_i\,(\Omega)\, ds + \int_V \sigma_i\, p_i\, \psi_i\,(\Omega)\, dr = \\ &\quad \frac{1}{4\pi}\int_V p_i\, \sigma_{s_i}\, dr \int_{4\pi} \psi\,(\Omega')\, d\Omega' + \int_V p_i\, S_i\,(\Omega) - \left\langle \int_\Gamma \left(n_i\cdot\Omega\right) \psi\,(\Omega)\, ds \right\rangle \end{aligned} \qquad \text{Eq. 28}$$

By applying the divergence theorem and taking the limit of the equation as V approaches zero

$$\frac{1}{\nu}\frac{\partial\left[p_i\psi_i(\Omega)\right]}{\partial t}+\Omega\cdot\bigtriangledown\left[p_i\psi_i(\Omega)\right]+\sigma_i\ p_i\psi_i(\Omega)=$$
$$\frac{\sigma_{s_i}}{4\pi}\ p_i\int_{4\pi}d\Omega'\psi_i(\Omega')+p_i S_i(\Omega)-\lim_{V\to 0}\left[\frac{1}{V}\left\langle\psi(\Omega)\int_{\Gamma}(n\cdot\Omega)\,ds\right\rangle\right] \qquad \text{Eq. 29}$$

This is the point where the derivation for the new coupled equations diverges from previous LP equation attempts. The last term is the difficult closure term that has been approximated in the past to attempt a satisfactory closure. By using a mesh with boundaries that do not change between realizations, there are no transitions between materials within any given cell over which the equation governs. This causes the last term to go to zero.

To further simplify the coupled equations we define

$$\widetilde{\psi}_i^n=p_i^n\cdot\psi_i^n=\left\langle\chi_i^n\psi_i\right\rangle \qquad \text{Eq. 30}$$

By using this definition in equation (30), the result looks almost exactly like equation (4) and the diamond difference derivation can be completed just as it was previously.

We will, therefore, go ahead and write an equation for the average flux in each material. Following the derivation from the DD S_N code:

$$\widetilde{\psi}_{m,i}^0=\left(\widetilde{\psi}_{m,i-\frac{1}{2}}^0+\frac{\Delta x}{2\mu}\right)\frac{\frac{\sigma_s^0}{2}\widetilde{\Phi}^0+S_i}{1+\sigma_t^0\frac{\Delta x}{2\mu}}$$
$$\widetilde{\psi}_{m,i}^1=\left(\widetilde{\psi}_{m,i-\frac{1}{2}}^1+\frac{\Delta x}{2\mu}\right)\frac{\frac{\sigma_s^1}{2}\widetilde{\Phi}^1+S_i}{1+\sigma_t^1\frac{\Delta x}{2\mu}} \qquad \text{Eq. 31, 32}$$

The corresponding angular flux on the opposite side is then updated for each material.

$$\widetilde{\psi}_{m,i+\frac{1}{2}}^0=2\widetilde{\psi}_{m,i}^0-\widetilde{\psi}_{m,i-\frac{1}{2}}^0$$
$$\widetilde{\psi}_{m,i+\frac{1}{2}}^1=2\widetilde{\psi}_{m,i}^1-\widetilde{\psi}_{m,i-\frac{1}{2}}^1 \qquad \text{Eq. 33, 34}$$

We define the angular flux entering the next cell as a percentage of the flux leaving the current cell.

$$\widetilde{\psi}^{0}_{m,(i+1)-\frac{1}{2}} = p_0\left(\widetilde{\psi}^{0}_{m,i+\frac{1}{2}} + \widetilde{\psi}^{1}_{m,i+\frac{1}{2}}\right)$$
$$\widetilde{\psi}^{1}_{m,(i+1)-\frac{1}{2}} = p_1\left(\widetilde{\psi}^{0}_{m,i+\frac{1}{2}} + \widetilde{\psi}^{1}_{m,i+\frac{1}{2}}\right) \qquad \text{Eq. 35, 36}$$

We can say this because we began with

$$\widetilde{\psi}_{i,m} = \widetilde{\psi}^{0}_{i,m} + \widetilde{\psi}^{1}_{i,m} \qquad \text{Eq. 37}$$

This step simply couples the two equations by redistributing the particles between the two materials based on the material distribution probabilities.

Once, again we sweep through the mesh, calculate the scalar fluxes, and test for convergence where

$$\widetilde{\Phi}_i = \sum_{m=1}^{N}\left(w_m \cdot \left(\widetilde{\psi}^{0}_{i,m} + \widetilde{\psi}^{1}_{i,m}\right)\right) \qquad \text{Eq. 38}$$

4 Results

In this chapter, we present the results of various test problems that demonstrate the effectiveness of the mesh based BSM model in comparison with the brute force benchmarks.

Results from filling the mesh will be covered showing that the cells were filled randomly and evenly. Next the results of the distribution tools, the CLD and the CTP will be shown. These will focus on achieving a Markovian distribution. Next, the SN code will be compared against analytical solutions to verify that correct answers are achieved through use of the code. Finally, the coupled code will be matched against the “brute force” method in several cases.

4.1 Creating the mesh

The first set of test problems is designed to determine whether the realizations of the statistics are being created properly.

A 5x5x50 mesh was used to generate realizations based on the algorithm described in chapter (3.1). The results were then normalized using the largest tally, so that if every cell were filled the same number of times, each cell would have a value of unity.

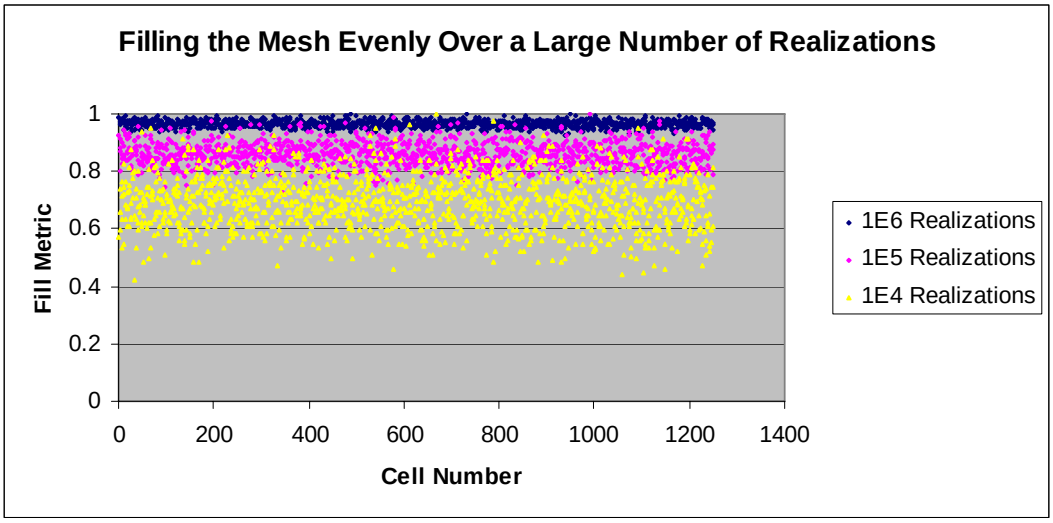

Figure 3 - Graph of Metric for Filling Mesh Evenly

Figure 3 clearly shows that the distribution of material is homogeneous; increasing the number of realizations in the calculation causes the metric to converge to a value of unity.

The second set of test problems is designed to investigate the chord length distributions obtained in a variety of realization generation approaches.

The process starts with a long thin mesh of 3x3x50 cells, as seen in figure (4). Each cell is a cube with a side length of 0.1 cm. The mesh is filled with 10% of material 0 and 90% of material 1 and the CLD is calculated. The mesh is then expanded to 9x9x 50 cells, maintaining cell dimensions and fill percentages and the CLD is calculated. 15x15x50, 25x25x50, and 50x50x50 meshes are also considered.

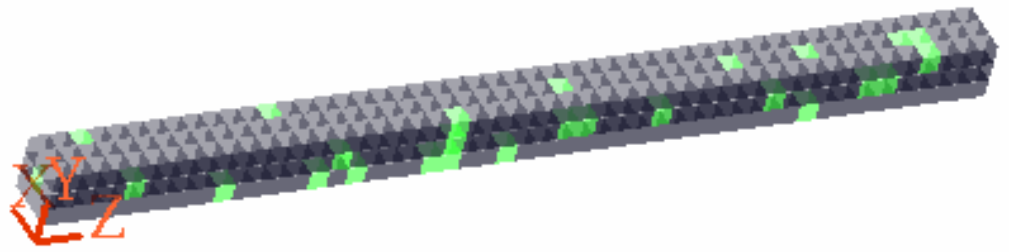

Figure 4 – 3x3x50 Mesh

Next, the aspect ratio of the problem was changed by flattening the previous mesh arrangement. The same cell sizes and fill fractions were used, but the mesh dimensions used were 15x9x50 and 15x3x50. Figure (5) shows a flattened mesh produced by varying the aspect ratio of the problems.

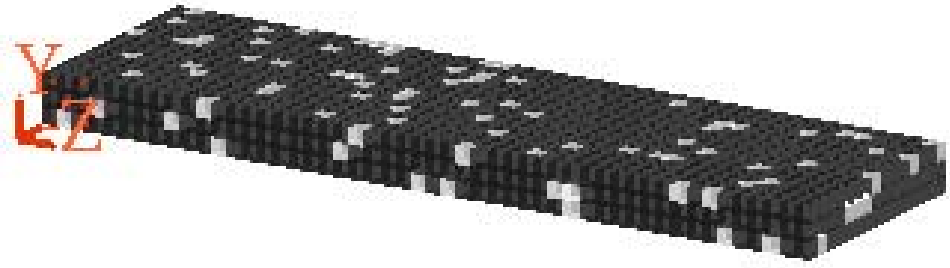

Figure 5 – 15x3x50 Mesh

Finally, using the 15x15x50 mesh, the CLD was calculated using material 0 fill percentages of 10%, 25% and 50%. Figure 6 shows the mesh used for calculating a CLD with a 50% fill.

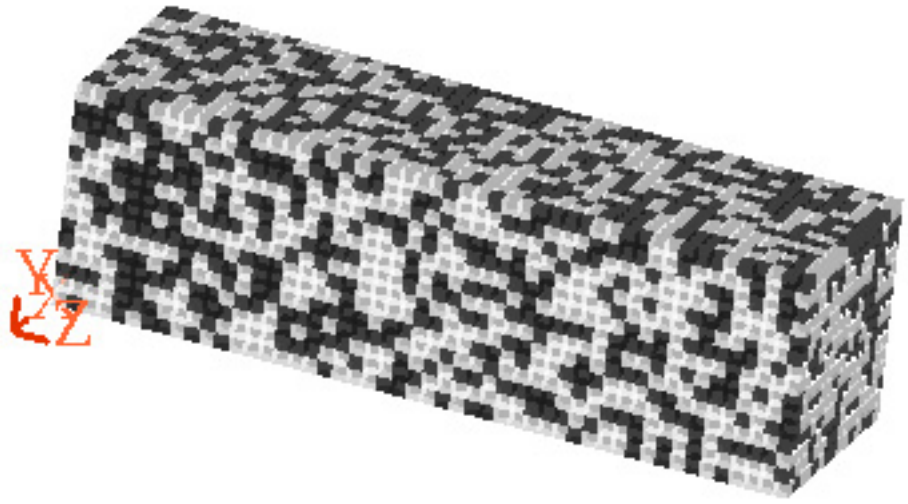

Figure 6 – 15x15x50 Mesh with 50% Fill

Each of the CLD calculations used 1E6 chords in determining the distribution.

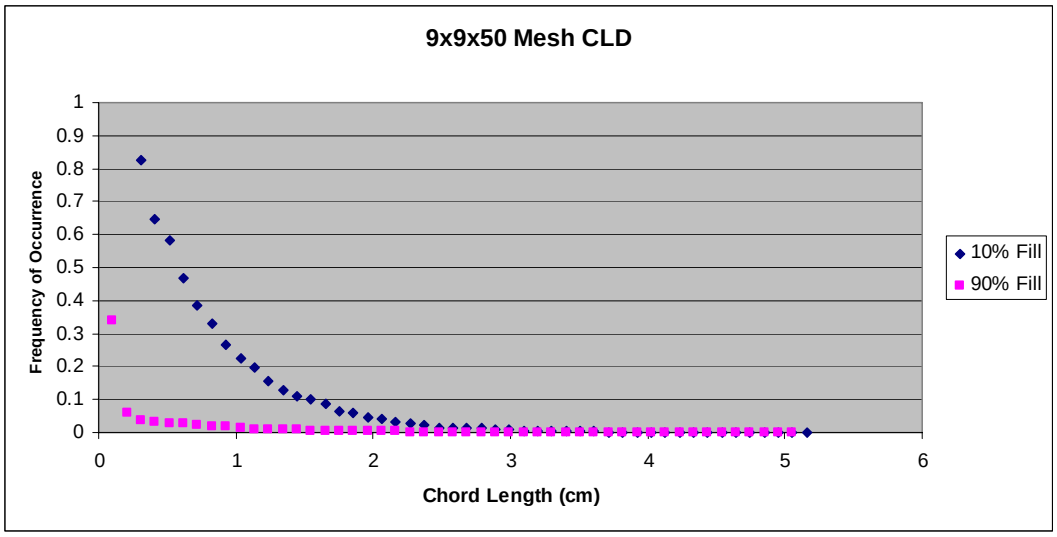

Figure 7 – 9x9x50 Mesh CLD

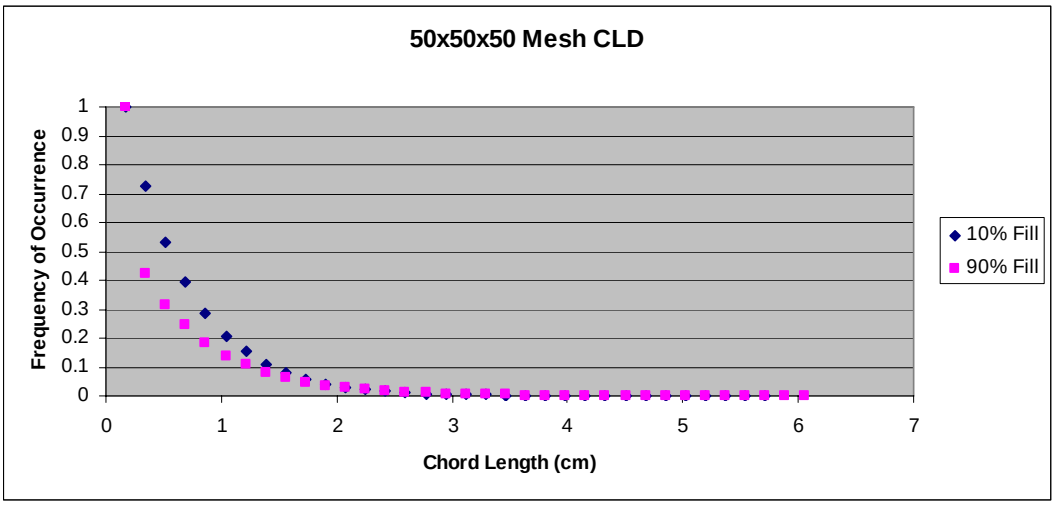

Figure 8 - 50x50x50 Mesh CLD

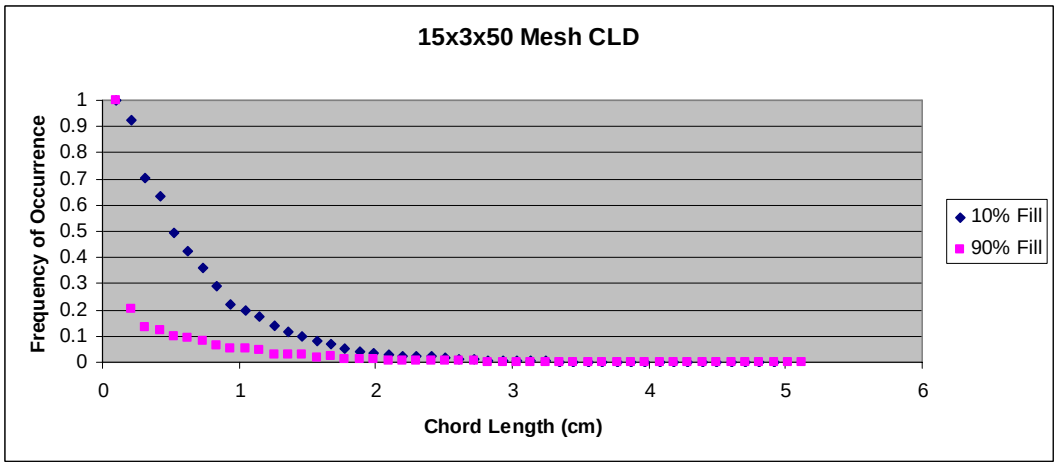

Figure 9 – 15x3x50 Mesh CLD

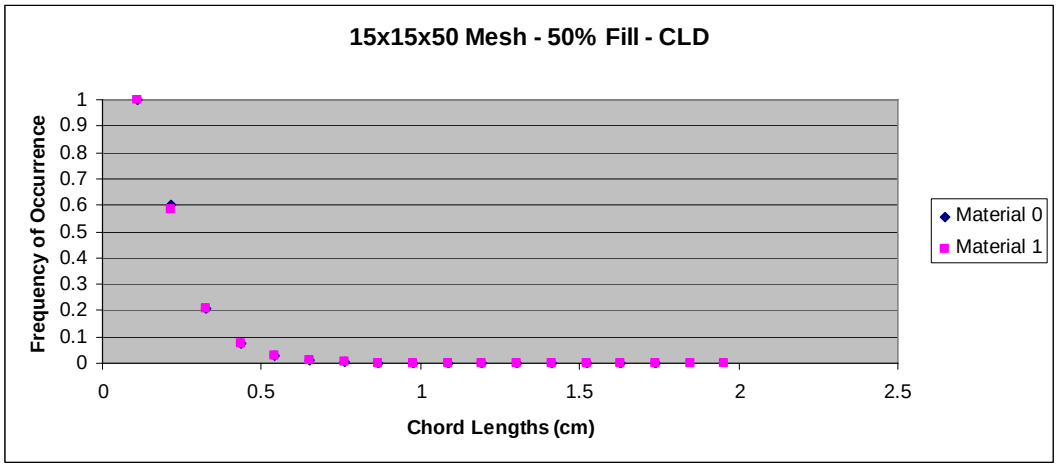

Figure 10 – 15x15x50 Mesh CLD with 50% Fill

Table 1 – Exponential Fits for Different Mesh Sizes with Material 0

Material 0 (10% Fill)		
	λ (cm)	R^2
50x50x50	2.1430	0.9906
25x25x50	2.3250	0.9729
15x15x50	2.0680	0.9829
9x9x50	2.0864	0.9164
3x3x50	2.4572	0.9395

Table 2 - Exponential Fits for Different Mesh Sizes with Material 1

Material 1 (90% Fill)		
	λ (cm)	R^2
50x50x50	1.7343	0.9889
25x25x50	1.9363	0.9638
15x15x50	1.7564	0.9571
9x9x50	1.5900	0.9745
3x3x50	1.7342	0.9457

Table 3 – Exponential Fits for Different Fill Fractions

Curve Parameters		
Fill %	λ_1 (cm)	λ_2 (cm)
10	2.0800	1.7564
25	4.2056	4.3097
50	8.6982	8.3832

Tables (1), (2,), and(3) show that all of the tested mesh configurations have chord length distributions that can be fit to exponential curve with R^2>0.9 (nearly all

with R^2 >0.95). The curve fit parameter is the mean chord length, found in the definition of an exponential distribution, equation (1). These results indicate that exponential chord length distributions are applicable to these problems. The change in the CLDs due to the shape of the mesh are small (maximum relative error of less than 18%); larger problems tend to have distributions that are closer to an exponential curve. The fill percentage has a significant impact, however, approximately doubling λ as the fill percentage doubled.

We have also investigated the homogeneity of the process of generating realizations by calculating CTPs. This data is also used in the mesh based coupled BSM model. A sampling of 1E8 3x3x3 meshes shows the probabilities where material 0 represented 10% of the volume and material 1 represents 90%. The probabilities from the 6 surfaces were averaged (since there is only one interior cell, there are only six surfaces on which material transitions occur) and can be seen in table (4).

Table 4 – CTP for a 10/90 Fill Fraction

Material Transition	Probability
10 to 10	0.00855
10 to 90	0.10219
90 to 10	0.10219
90 to 90	0.78707

4.2 Brute Force Benchmarks

Before generating brute force solutions, it is important to verify the code is working by comparing a single solution generated with the code to an answer that is known to be correct. Analytic solutions are known to several 1D problems and by simulating a 1D problem with the 3D code, verification can be performed.

One well known analytical problem is the 1D pure absorber. In order to use the 3D code to solve this problem, a mesh of 50 cubes lined up down the z-axis is defined. Each cube is 0.1 cm along the edge. The problem is driven on the z=0 side of the problem with an incident source strength of 3.0 and all other problem boundaries

are vacuum. All angles used are normal to the face so that the only leakage that will occur at the far end of the problem. The problem is filled with a single material that is purely absorbing where $\sigma_a=\sigma_t=2.0$.

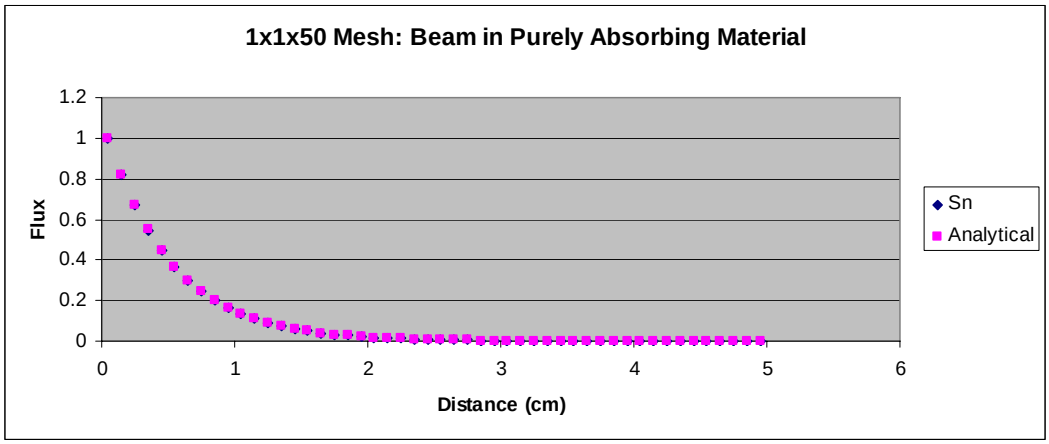

Figure 11 – 1D Beam in a Pure Absorber

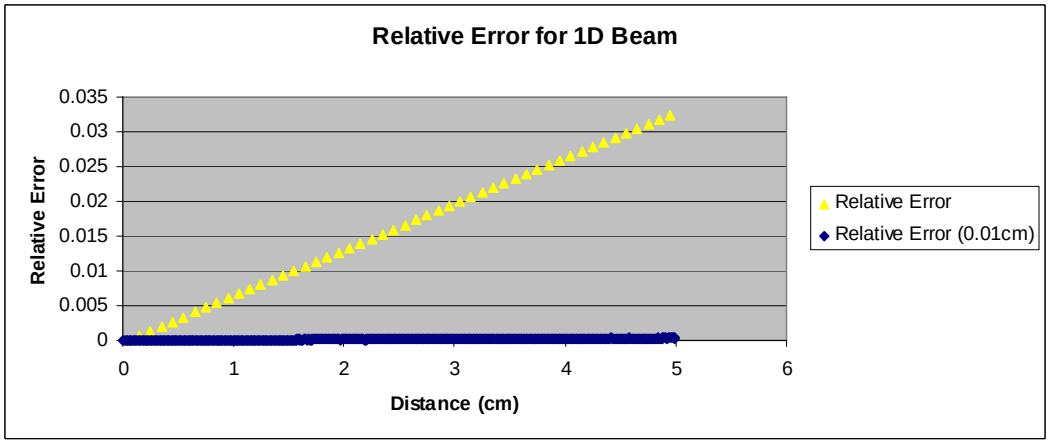

Figure 12 – Relative Error for a 1D Beam in a Pure Absorber

With an R^2 value of unity, the exponential regression of the data gives

$$\Phi(z)=e^{-2.0\cdot z}\ , \qquad \text{Eq. 39}$$

the expected analytical solution.

Note that the relative error increases linearly with distance as the error caused by the diamond differencing compounds. This error is expected and can be reduced by shrinking the cell size; figure 12 shows the relative error from the same

problem, but with cell sizes reduced by an order of magnitude. This concept was introduced and derived earlier, using equations (19), (20), and (21).

Next, we use multiple angles with a standard S_4 angular set. The remaining problem specifications are the same as those in the previous problem. The analytic result can be found as

$$\Phi(z) = \sum_{\mu} e^{-\frac{\sigma_c z}{\mu}} \qquad \text{Eq. 40}$$

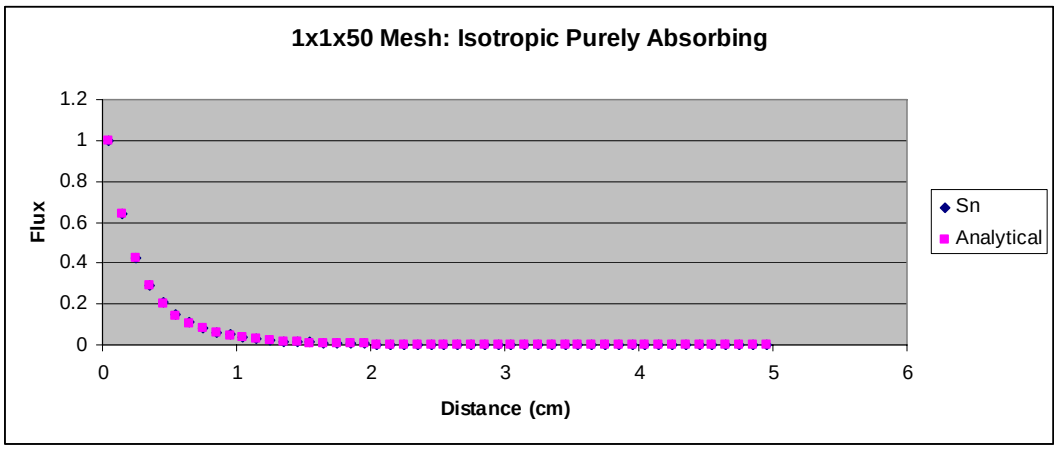

Figure 13 – 1D Pure Absorber with an Isotropic Source

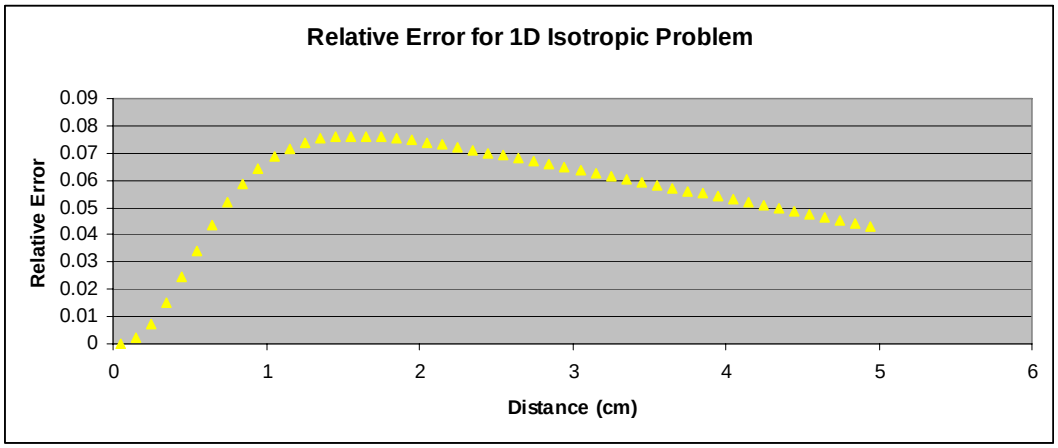

Figure 14 – Relative Error for 1D Pure Absorber with an Isotropic Source

Once again, we see that the answers agree. The change in the shape of the relative error curve is caused by the effects of the angular quadrature and is discussed in more detail later in the thesis. Once again, though not shown, the magnitude of this error is reduced by a reduction in cell size.

4.3 Mesh Based BSM Coupled Transport

Previous efforts at coupled transport have worked well in certain 1D problems. Results are typically compromised when scattering is involved. Many researchers have speculated that coupled equations with scattering should produce good results in 3D, although these results have not yet been achieved.

Three dimensional results can be difficult to visualize without an interactive environment. In order to deal with these difficulties, two different methods of graphical display will be used to interpret the test problem results. All the test problems will be set up in a similar fashion to the 1D case for ease of comparison and understanding.

If one can imagine a stack of square plates along the z-axis, one could view the average of each plate from the side. A plate can also be pulled from the stack to view the flux in the xy planes. The plots are constructed in this fashion so that the familiar scatter plot used in 1D comparisons can be used to view the results along the z-axis. Similarly, surface plots that are commonly used to view 2D problems are used in each slice of the problem for a visualization in the x and y directions.

For each problem, the slice averaged flux and the slice averaged relative error will be shown, followed by 2D plots of the relative error between the coupled method and the brute force method in slices at 10 cells, 30 cells, and 50 cells (the last slice) into the problem. Finally, the flux will be shown for slice 50, the farthest plane of cells from the source for both the brute force method and the coupled method.

The following types of test problems are considered:

1. Reflecting boundaries with purely absorbing materials

2. Reflecting boundaries with a background scattering material.
3. Vacuum boundaries with purely absorbing.
4. Vacuum boundaries with scattering
5. Atomic Mix Limit
6. Various Fill Percentages

The problems all use the same cross sections sets and use the same 10%/90% fill ratios. These cross sections were chosen so that the problems would be difficult to solve. The absorption cross-sections were chosen to be several orders of magnitude apart. The scattering material was chosen to be highly scattering. It is hoped that these "worse case" scenarios will allow for a reduction in the number of problems needed in order to show the effectiveness of the method.

Table 5 – Cross Sections for Absorbing Problems

Absorbing Problems		
Cross Sections	10% Fill	90% Fill
Σc	2.0	0.002
Σt	2.0	0.002

Table 6 – Cross Sections for Scattering Background Problems

Scattering Problems		
Cross Sections	10% Fill	90% Fill
Σc	2.0	1.5
Σt	2.0	2.0

Each of the meshes is 5x5x50 cells. In the reflecting problems, each cell is a cube of 0.1 cm on a side. The problems with vacuum boundaries, however, change the shape of the cell to reduce leakage out of the sides of the problem that result in negative fluxes. In these problems the length of the cell along the z-axis is reduced by one order of magnitude.

Similar to the 1D benchmarks, the problem is driven by an isotropic source, where each incident angular flux on the z=0 plane has a strength of 3.0.

The first problem is that with absorbing materials and reflecting boundaries. For the brute force method 5000 realizations were averaged.

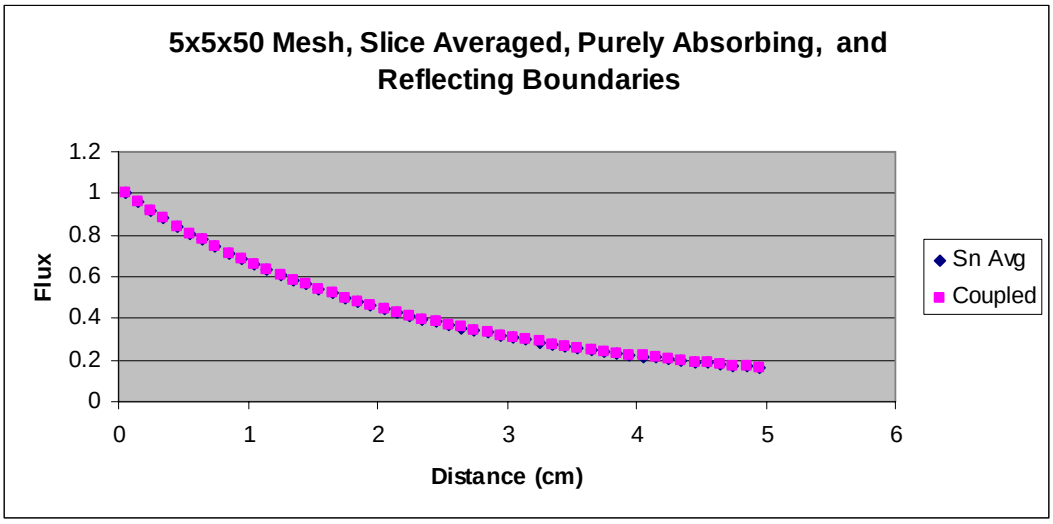

Figure 15 – Slice Averaged Pure Absorber with Reflecting Boundaries

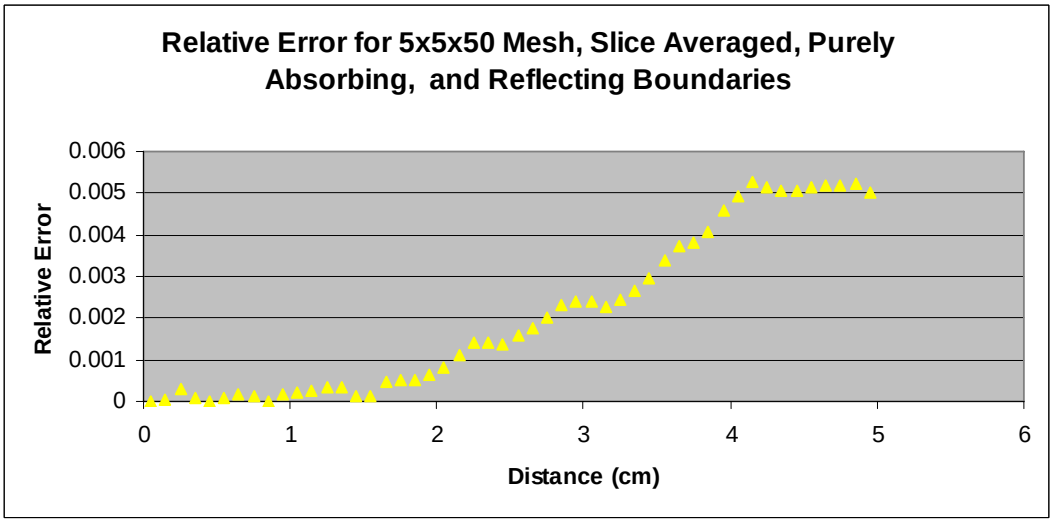

Figure 16 – Relative Error for Slice Averaged Pure Absorber with Reflecting Boundaries

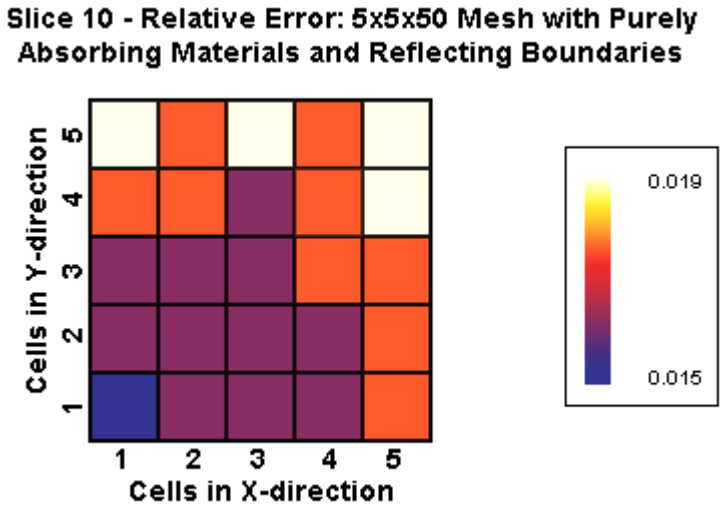

Figure 17 – Relative Error for Slice 10 of Pure Absorber with Reflecting Boundaries

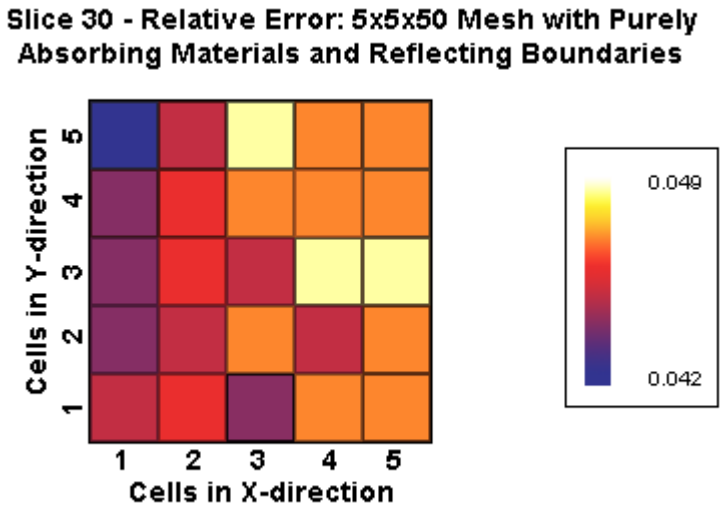

Figure 18– Relative Error for Slice 30 of Pure Absorber with Reflecting Boundaries

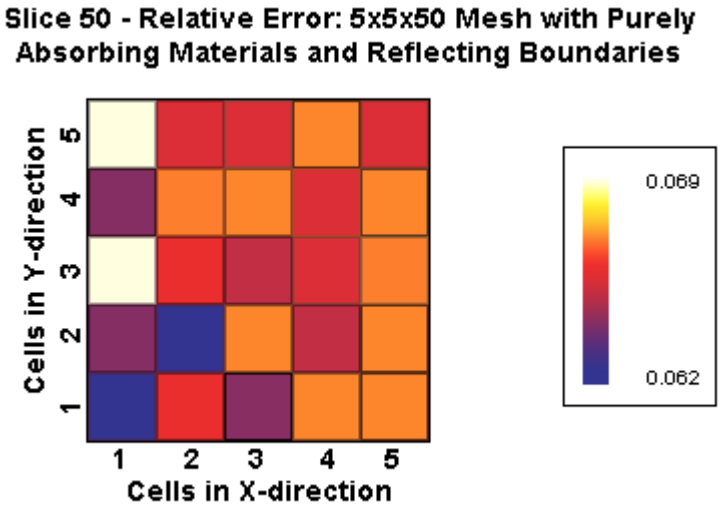

Figure 19 – Relative Error for Slice 50 of Pure Absorber with Reflecting Boundaries

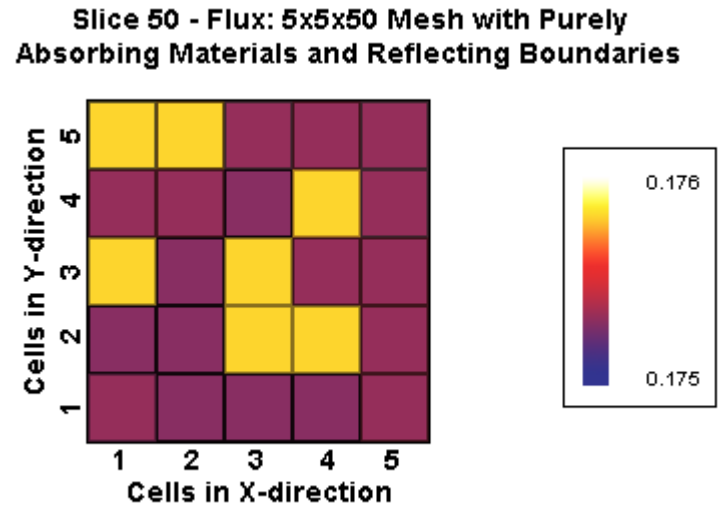

Figure 20 – Brute Force Method: Slice 50 of Pure Absorber with Reflecting Boundaries

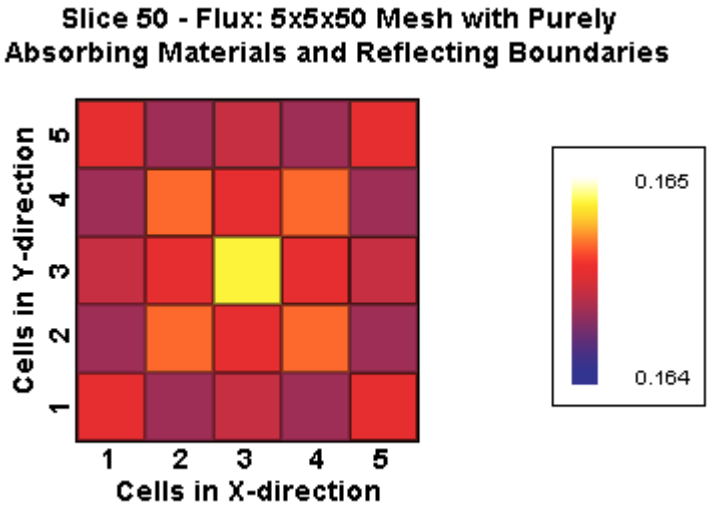

Figure 21 – Coupled Method: Slice 50 of Pure Absorber with Reflecting Boundaries

The next problem of interest is the same as the previous, except that the scattering materials cross section set is used and for the brute force method 10000 realizations are averaged.

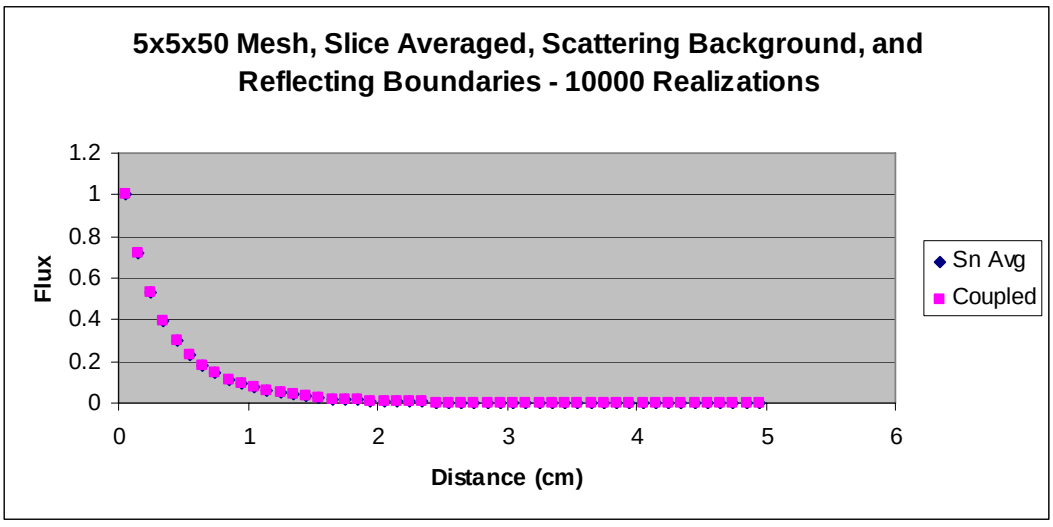

Figure 22 – Slice Averaged Scattering Background with Reflecting Boundaries

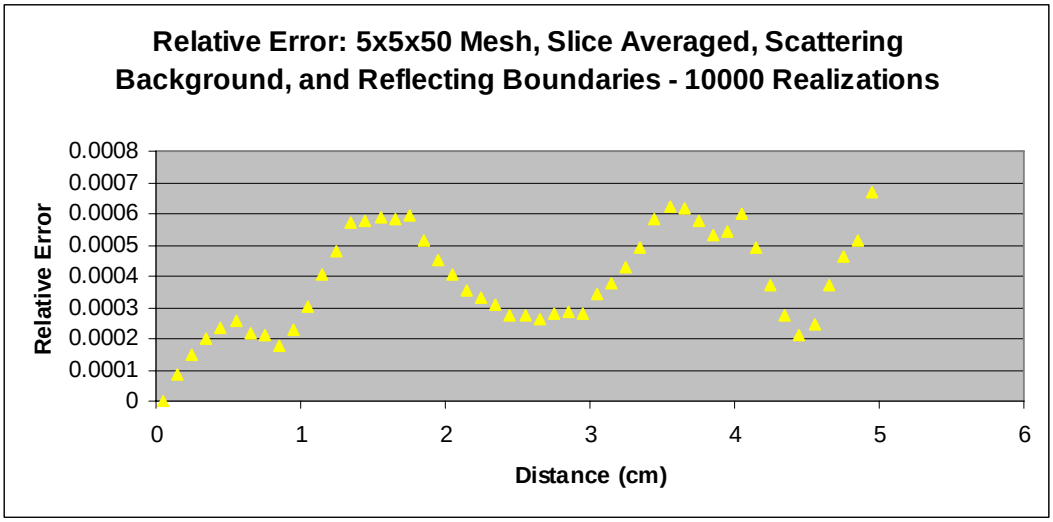

Figure 23 – Relative Error for Slice Averaged Pure Absorber with Reflecting Boundaries

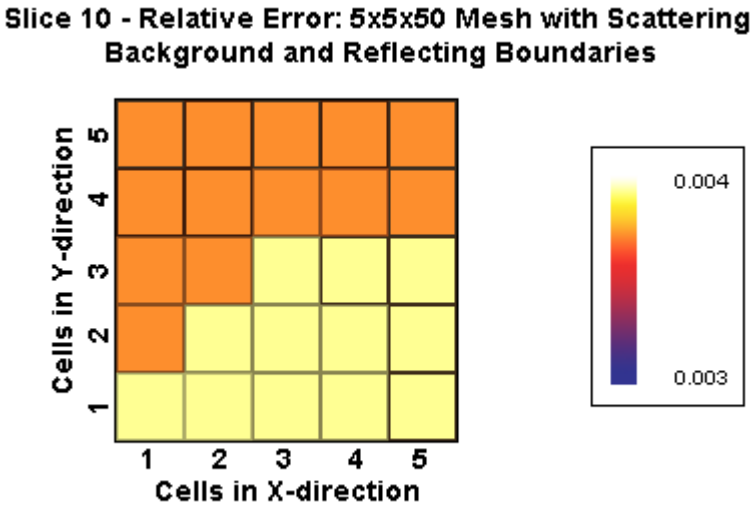

Figure 24 – Relative Error for Slice 10 of Scattering Background with Reflecting Boundaries

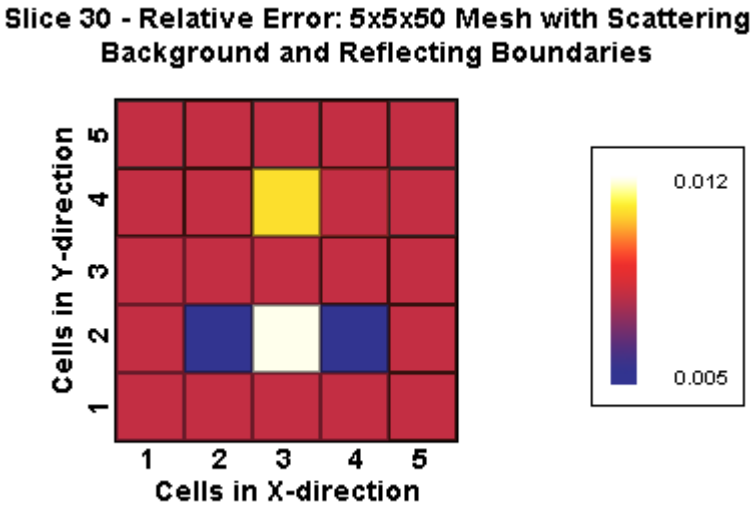

Figure 25 – Relative Error for Slice 30 of Scattering Background with Reflecting Boundaries

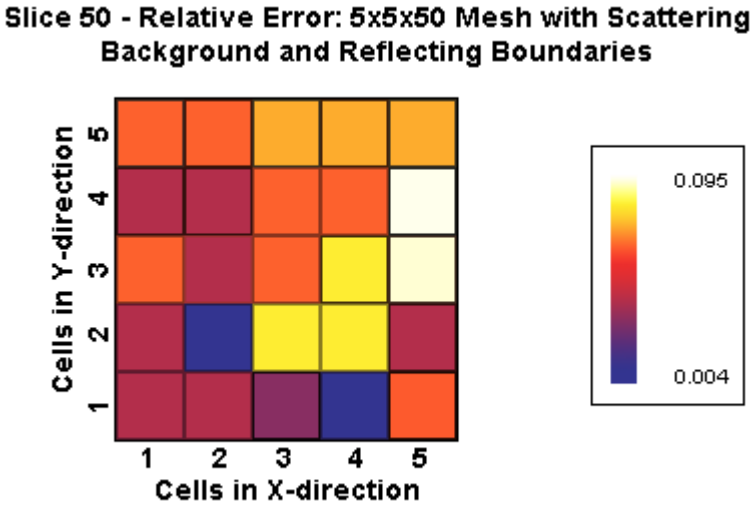

Figure 26 – Relative Error for Slice 50 of Scattering Background with Reflecting Boundaries

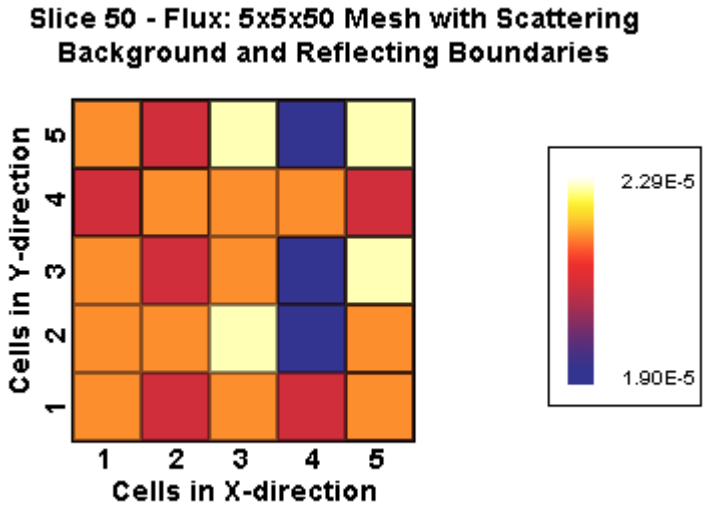

Figure 27 – Brute Force Method: Slice 50 of Scattering Background with Reflecting Boundaries

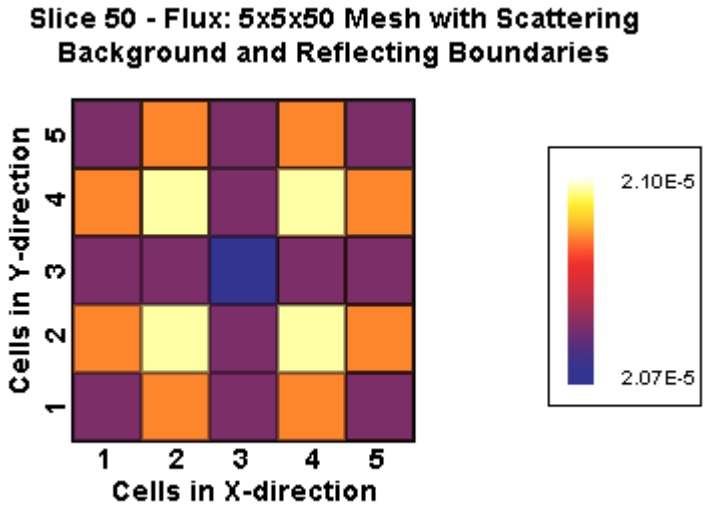

Figure 28 – Coupled Method: Slice 50 of Scattering Background with Reflecting Boundaries

The mesh for the third problem consists of 5x5x50 cells. Each cell, is 0.1 x 0.1 x 0.01 cm, with the shortest dimension lying along the z-axis. Vacuum boundaries are used on all sides of the mesh and the problem is driven on the z=0 face by an

isotropic angular flux of 3.0. The absorption cross section set listed in Table 5 is used for the materials in a 10%/90% mix.

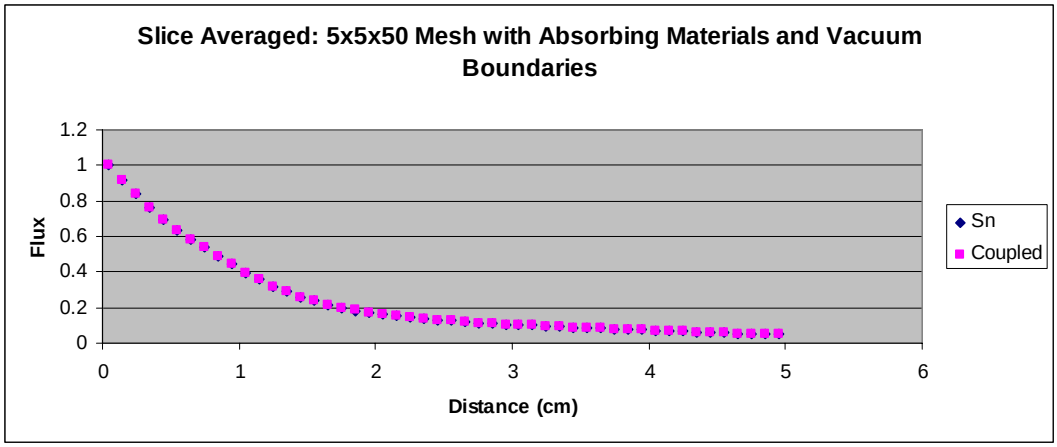

Figure 29 – Slice Averaged Pure Absorber with Vacuum Boundaries

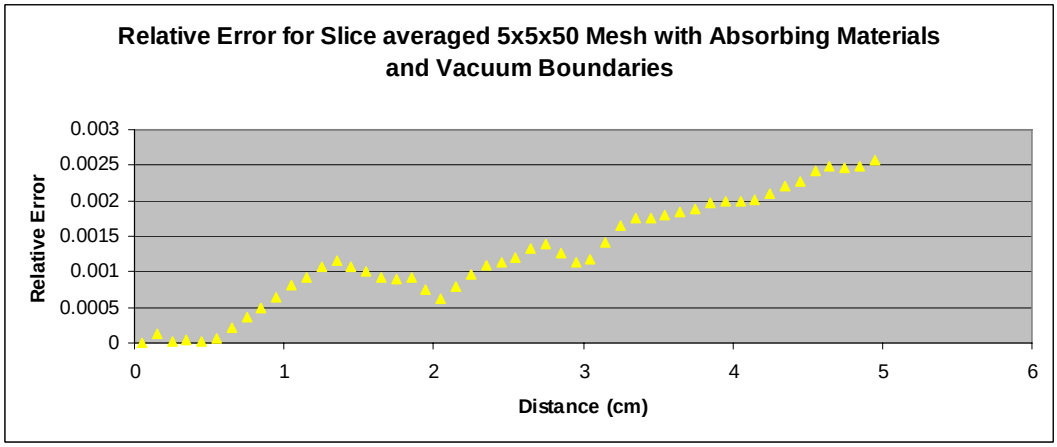

Figure 30 – Relative Error for Slice Averaged Pure Absorber with Vacuum Boundaries

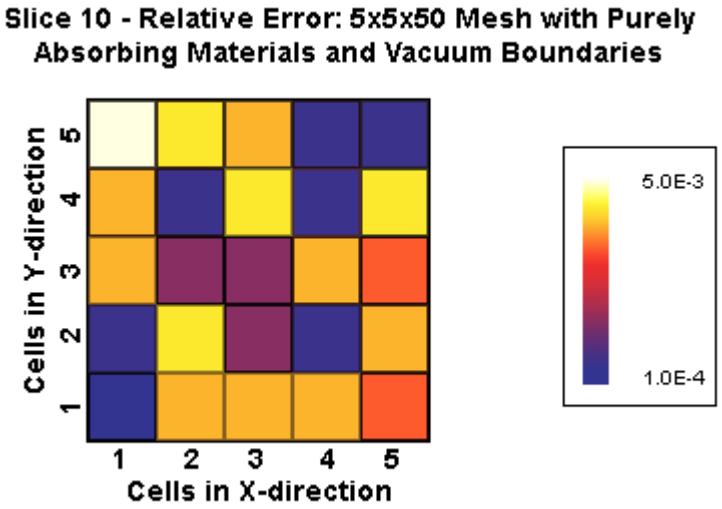

Figure 31 – Relative Error for Slice 10 of Pure Absorber with Vacuum Boundaries

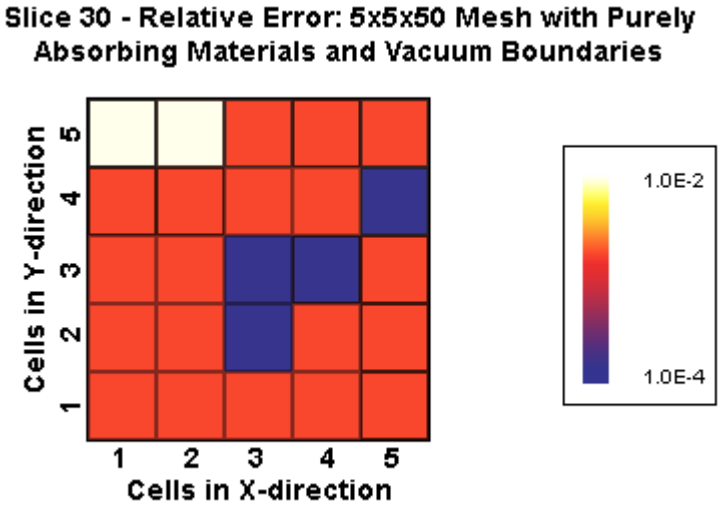

Figure 32 – Relative Error for Slice 30 of Pure Absorber with Vacuum Boundaries

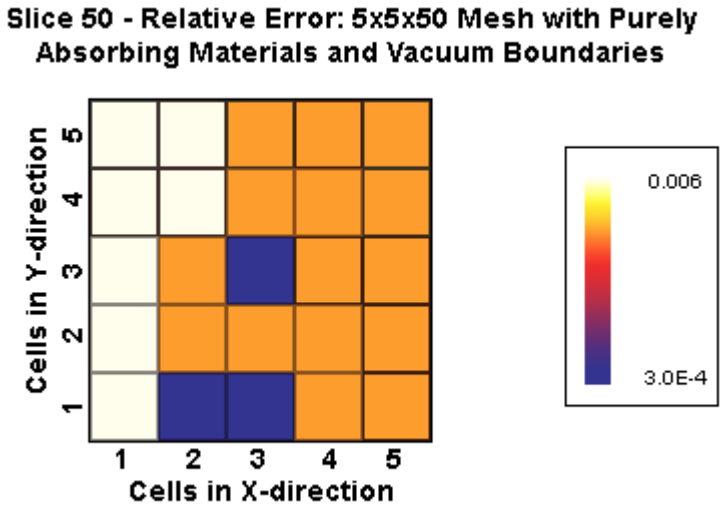

Figure 33 – Relative Error for Slice 50 of Pure Absorber with Vacuum Boundaries

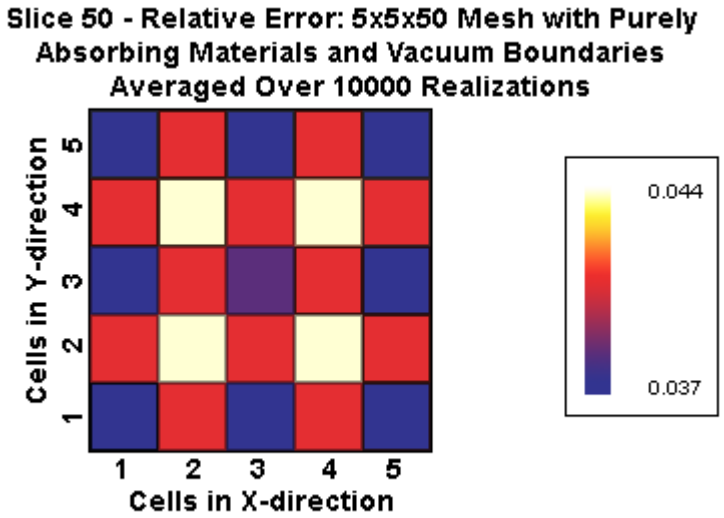

Figure 34 – Brute Force Method: Slice 50 of Pure Absorber with Vacuum Boundaries

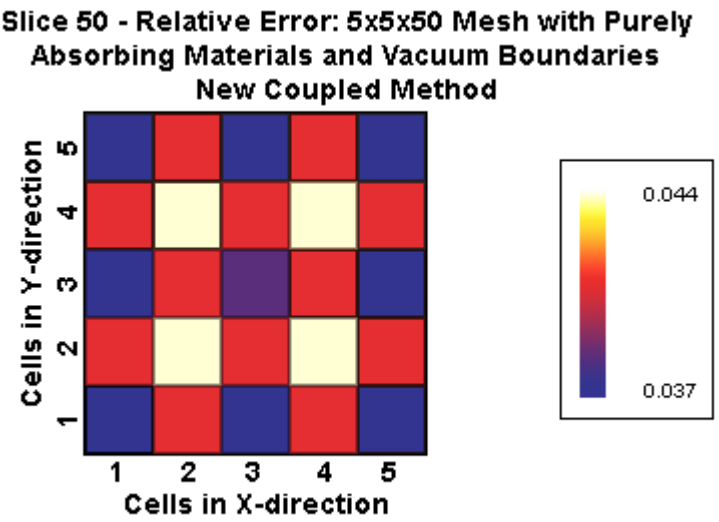

Figure 35 – Coupled Method: Slice 50 of Pure Absorber with Vacuum Boundaries

The fourth problem is the same as the third, but the scattering cross section set listed in Table 6 is used instead.

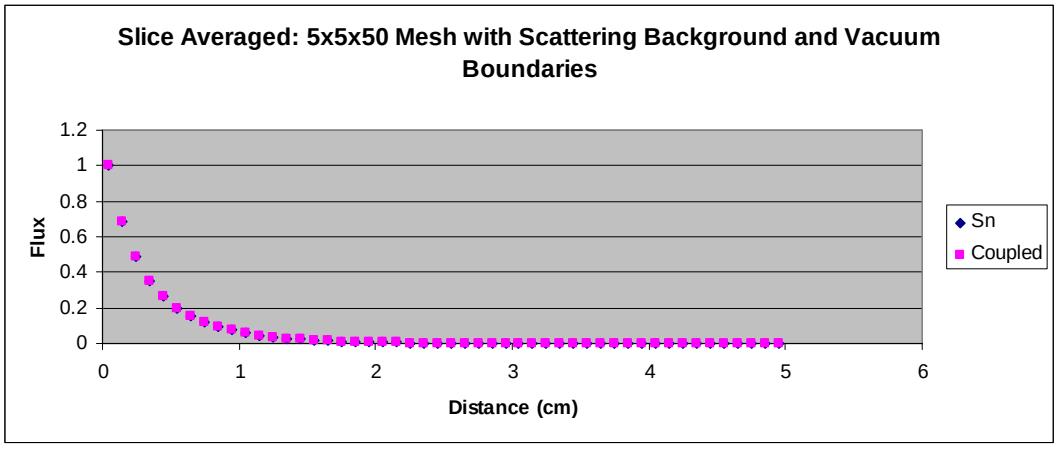

Figure 36 – Slice Averaged Scattering Background with Vacuum Boundaries

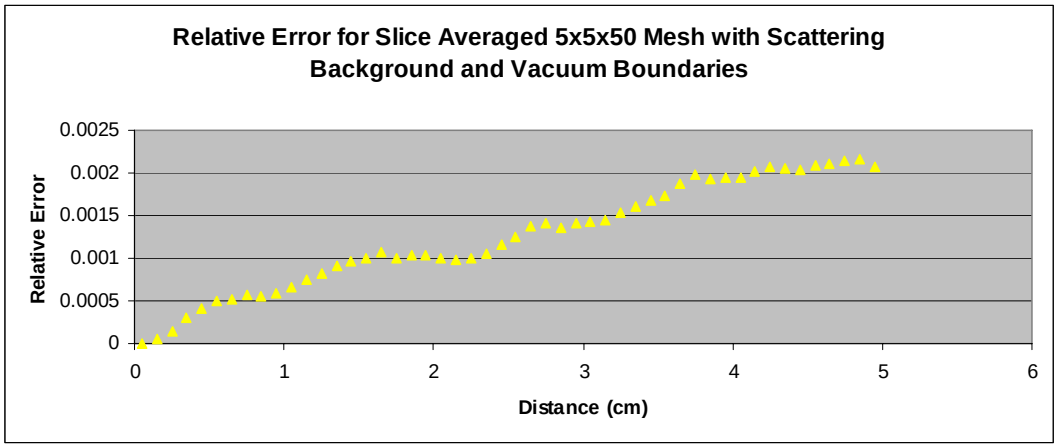

Figure 37 – Relative Error for Slice Averaged Scattering Background with Vacuum Boundaries

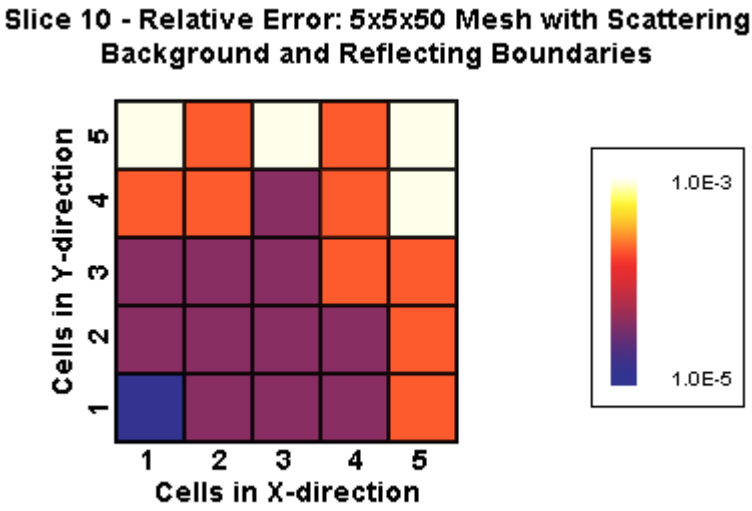

Figure 38 – Relative Error for Slice 10 of Scattering Background with Vacuum Boundaries

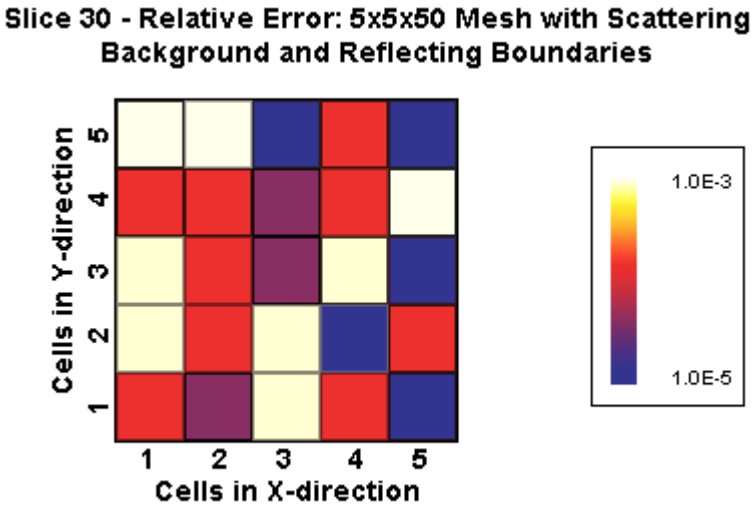

Figure 39 – Relative Error for Slice 30 of Scattering Background with Vacuum Boundaries

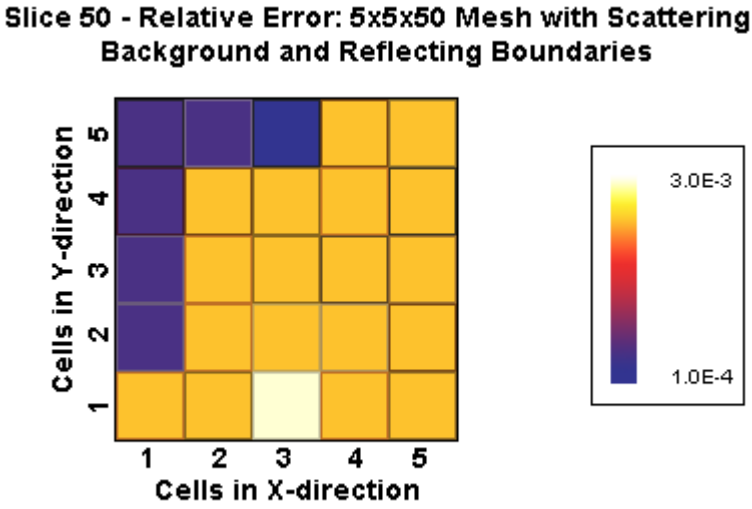

Figure 40 – Relative Error for Slice 50 of Scattering Background with Vacuum Boundaries

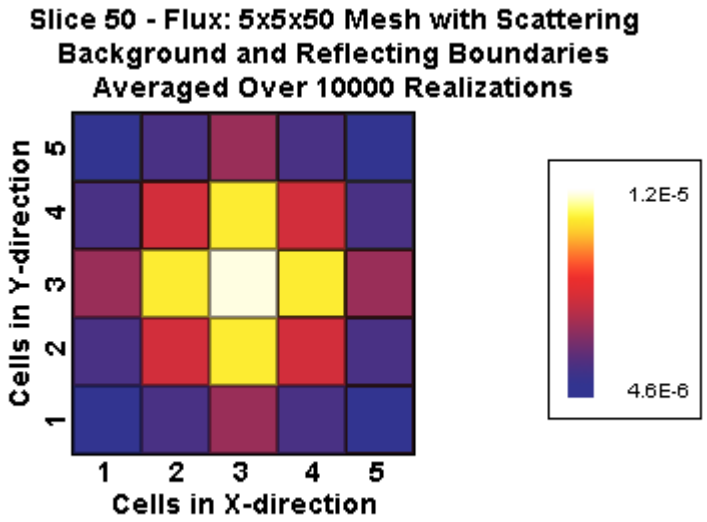

Figure 41 – Brute Force Method: Slice 50 of Scattering Background with Vacuum Boundaries

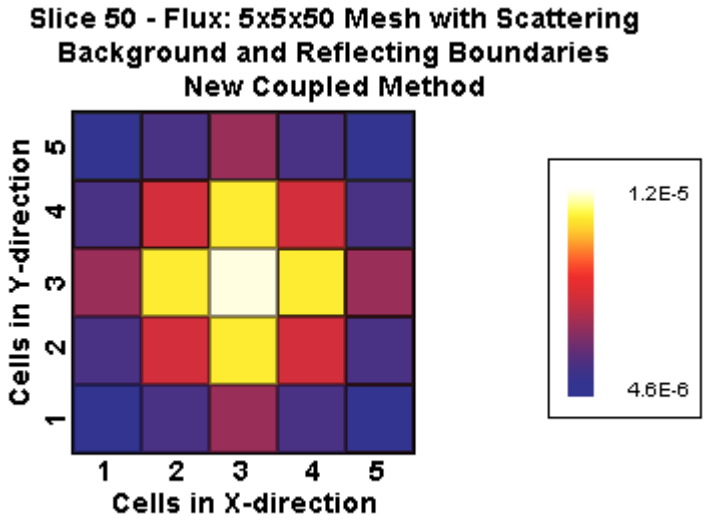

Figure 42 – Coupled Method: Slice 50 of Scattering Background with Vacuum Boundaries

The next problem of interest is the atomic mix limit problem. If the cells in the mesh are small enough and the mesh is filled with two purely absorbing materials with different cross sections, the coupled method should produce the same solution as a homogenized analytic solution.

The 1x1x50 cell mesh is comprised of cubic cells measuring 0.0001 cm on a side. Similar to previous 1D problems, four of the sides are reflecting, while the planes perpendicular to the z-axis are vacuum boundaries. The problem is driven by an isotropic angular flux of 3.0 and two pure absorbers are used: the 10% fill has a σ_a of 20.0 and the 90% fill material has a σ_a of 0.002.

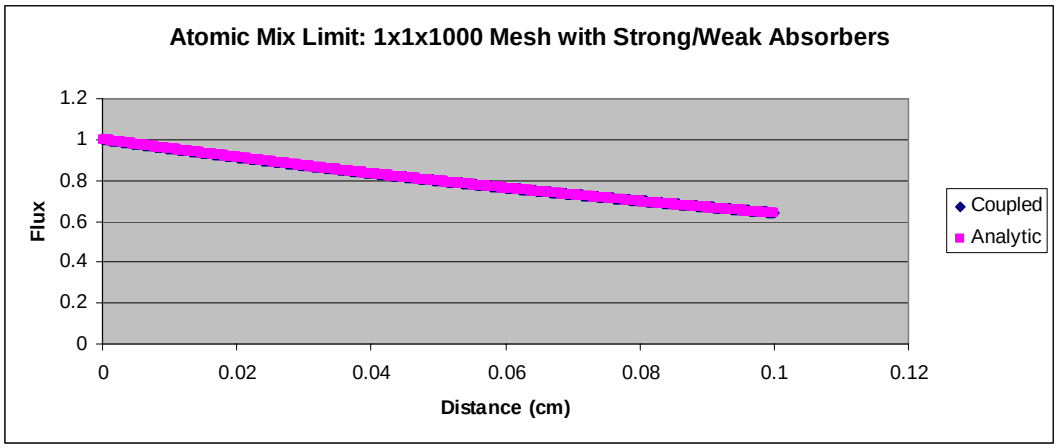

Figure 43 – Atomic Mix Limit of Pure Absorbers

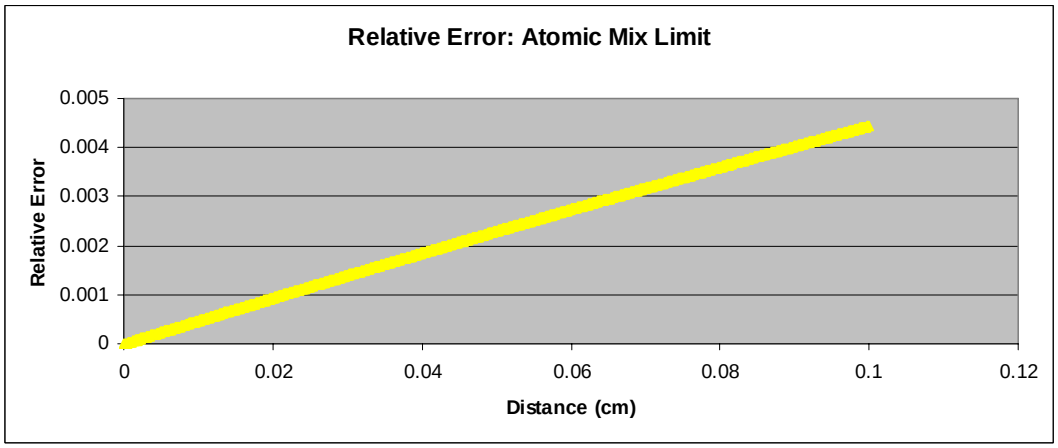

Figure 44 – Relative Error of Atomic Mix Limit of Pure Absorbers

Finally, a 5x5x50 mesh was filled with different fill percentages of materials, otherwise the two problem configurations were the same as the vacuum boundary problems run previously. The solutions of the brute force method were averaged over 1E4 realizations.

Table 7 - Maximum Relative Error for Different Fill Percentages

Maximum Relative Error					
	10%	20%	30%	40%	50%
Absorbing	0.006778	0.003217	0.001587	0.001989	0.002692
Scattering	0.003118	0.002108	0.002528	0.003581	0.00216

5 Discussion

Discussing the results from the previous section may aid in arriving at the appropriate conclusions over the data. Some of the problems need to be qualified as to what they show.

Figures (11) and (12) show that the diamond differencing reproduces the analytic solution in a pure absorbing medium with the expected error. The error grows linearly with distance into the problem and is reduced when the cell size is reduced. The error induced is exactly what can be expected from a diamond difference method and was derived in the methods section.

Figures (13) and (14) show solutions using the S4 angular quadrature which suffer from ray effects. While the best way to avoid the ray is to use quadrature sets with many more angles, it is computationally expensive. Using sets with a few more angles could have shown the ray effect peaks in the error function change and would have been helpful in proving the method, but modifying the code to do so would have been too time intensive.

The problems with reflecting boundaries show a lack in the number of realizations solved and averaged. The reflecting problems were very time consuming to solve due to slow convergence, as discussed in section 3.3. For this reason, not as many were run and the results for the brute force method slightly suffered. The flux distributions in the last slices of the brute force method reflecting problems, figures (19) and (26), lack in symmetry. This symmetry is found, however, in the fluxes for the coupled method of the same problems, figures (20) and (27). This symmetry is expected. The lack of a resolved average in the brute force method can be seen throughout both problems, as shown in the relative error plots, figures (19) and (26), which are not yet smooth functions. While more realizations are needed in the brute force method, the relative error is still very small, as can be seen in the plots of the slices.

Figures (29) and (36) show that the relative error functions in the vacuum problems are much smoother. The vacuum problems were much quicker to converge, and as a result, more realizations were averaged. The effects can also be seen in the fluxes in the last slices, which very nearly match each other in the respective problems (Figures 33, 34, 40 and 41).

The next objective was to match the atomic mix limit. Figures (42) shows that the results match extremely well to the analytic solution. Figure (43) not only echoes this through the display of small relative errors, but also shows the same linear buildup of error inherent in the diamond differencing scheme. Although though the atomic limit in the scattering is not shown, it was investigated and the results were very similar.

Table 7 illustrates that, since there is no trend in the data points, there is no connection between the effectiveness of the new coupled method and the fill percentages of the materials in the problem.

Results were taken from benchmarks produced by Adams et. al. in 1D planar cases [**12**]. The current was calculated at either end of a 1D Markovian distribution of materials. Here we look at several of the worst cases – those which involved high scattering materials.

Table 10 in their paper shows that the relative error between the LP equations result and the brute force result in the far end of a 10 cm long problem was 77.4%. In similar problems, relative errors of 24%, 24.3%, and 30% were seen. These problems had a pure absorber for material 0 and high scattering material 1. The problems in this thesis were designed to look much like these for comparison of the methods.

The computational time of one iteration of the coupled method is similar to that of one iteration of a standard S_N code. There is slightly more math being done per sweep, as two sets of equations are being solved rather than one. The number of iterations per problem solution were also similar. Some coupled solutions required slightly ore or less iterations to reach convergence, but no trend was observed with the number of problems examined. However, when one takes into account that only one solution of the coupled method is required versus thousands using the brute force method, it is greatly faster.

6 Conclusion

While an exact Markovian distribution of materials is not achievedusing our approach for generating realizations, the CLDs did resemble an exponential curve and fit with R^2>0.95 for most problems. The shape of the mesh had little impact on the exponential curve fit, but increasing the number of cells in the mesh did seem to make the CLD more exponential in shape. The fill percentage did have a large effect on the parameters in the exponential fit, however.

The mesh was shown to be populated correctly by tallying the number of times each cell was filled with each material. The CTPs corroborated this conclusion by showing that the mesh was being filled to the correct percentages and that the distribution was homogeneous.

By using a mesh, it was shown that the difficult closure term from past coupled transport methods is not present. The new mesh based coupled BSM transport equations are simpler, with material coupling occurring only on cell surfaces. These equations are robust and conservative.

Solutions from the coupled equations were then compared to those from the brute force method. It was shown that the coupled equations performed well in absorbing problems and in scattering problems. They were also shown to solve an atomic mix problem correctly, matching an analytical homogenized problem. In addition, changing the fill percentages of the materials did not affect the accuracy of the solutions produced by the new coupled method.

Relative errors of the fluxes calculated with the new coupled method were extremely low compared to previous attempts at coupled transport. The LP equations were shown to produce relative errors of up to 77%, while the new coupled method steadily produced relative errors of under 1%, much of which can be attributed to statistical variance.

Solving more problems by averaging over many more realizations would almost certainly show even lower errors than were calculated in this work. Future work would include exploring different material distributions and better differencing schemes than diamond differencing (linear discontinuous, characteristics, etc.).

Using different quadrature sets would also be a beneficial exercise. Interior sources were not used in any of the problems, although it is not expected that this would affect the accuracy of the new coupled method. Also, calculating the variance of the problem solutions would be valuable, as it is expected that the solutions most likely lie within the variance of each other.

7 Bibliography

1. E. E. Lewis and J. W.F. Miller, *Computational methods of neutron transport*, American Nuclear Society, Inc., 1993.
2. "Close encounters of the particle kind," *1663*, Los Alamos National Labs, Los Alamos, NM, 2008.
3. J. D. Densmore, T. J. Urbatsch, T. M. Evans and M. W. Buksas, *A hybrid transport-diffusion method for monte carlo radiative-transfer simulations*, Journal of Computational Physics **222** (2007), no. 2, 485-503.
4. T. L. Becker, A. B. Wollaber and E. W. Larsen, *A hybrid monte carlo-deterministic method for global particle transport calculations*, Nuclear Science and Engineering **155** (2007), no. 2, 155-167.
5. S. A. Turner and E. W. Larsen, *Automatic variance reduction for three-dimensional monte carlo simulations by the local importance function transform .1. Analysis*, Nuclear Science and Engineering **127** (1997), no. 1, 22-35.
6. G. A. Titov, *Statistical description of radiation transfer in clouds*, Journal of the Atmospheric Sciences **47** (1990), no. 1, 24-38.
7. T. S. Palmer and B. S. Ching, *A "Two-grid" Acceleration of binary stochastic mixture deterministic transport iterations in slab geometry*, Annals of Nuclear Energy **35** (2008), no. 1, 68-74.
8. G. C. Pomraning, *Small correlation length solutions for planar symmetry beam transport in a stochastic medium*, Annals of Nuclear Energy **23** (1996), no. 10, 843-861.
9. P. Boisse, *Radiative-transfer inside clumpy media - the penetration of uv photons inside molecular clouds*, Astronomy and Astrophysics **228** (1990), no. 2, 483-502.
10. G. C. Pomraning, *The effect of random material density on reactor criticality*, Nuclear Science and Engineering **108** (1991), no. 4, 325-330.
11. C. D. Levermore, G. C. Pomraning, D. L. Sanzo and J. Wong, *Linear transport-theory in a random medium*, Journal of Mathematical Physics **27** (1986), no. 10, 2526-2536.
12. M. L. Adams, E. W. Larsen and G. C. Pomraning, *Benchmark results for particle-transport in a binary markov statistical medium*, Journal of Quantitative Spectroscopy & Radiative Transfer **42** (1989), no. 4, 253-266.
13. D. Vanderhaegen, *Radiative-transfer in statistically heterogeneous mixtures*, Journal of Quantitative Spectroscopy & Radiative Transfer **36** (1986), no. 6, 557-561.
14. G. L. Olson, D. S. Miller, E. W. Larsen and J. E. Morel, *Chord length distributions in binary stochastic media in two and three dimensions*, Journal of Quantitative Spectroscopy & Radiative Transfer **101** (2006), no. 2, 269-283.
15. D. Vanderhaegen and C. Deutsch, *Linear radiation transport in randomly distributed binary-mixtures - a one-dimensional and exact treatment for*

the scattering case, Journal of Statistical Physics **54** (1989), no. 1-2, 331-360.

16. A. K. Prinja, *On the master equation approach to transport in discrete random media in the presence of scattering*, Annals of Nuclear Energy **31** (2004), no. 17, 2005-2016.
17. F. Graziani and D. Slone, "Radiation transport in 3d heterogeneous materials: Direct numerical simulation," *American Nuclear Society*, LLNL, New Orleans, 2003.
18. G. L. Olson, *Gray radiation transport in multi-dimensional stochastic binary media with material temperature coupling*, Journal of Quantitative Spectroscopy & Radiative Transfer **104** (2007), no. 1, 86-98.
19. G. C. Pomraning, *Renewal analysis for higher moments in stochastic transport*, Journal of Quantitative Spectroscopy & Radiative Transfer **57** (1997), no. 3, 295-307.
20. ---, *Statistics, renewal theory, and particle-transport*, Journal of Quantitative Spectroscopy & Radiative Transfer **42** (1989), no. 4, 279-293.
21. H. Frisch, G. C. Pomraning and P. F. Zweifel, *An exact analytical solution of a radiative-transfer problem in a binary mixture*, Journal of Quantitative Spectroscopy & Radiative Transfer **43** (1990), no. 4, 271-284.
22. C. D. Levermore, J. Wong and G. C. Pomraning, *Renewal theory for transport processes in binary statistical mixtures*, Journal of Mathematical Physics **29** (1988), no. 4, 995-1004.
23. G. C. Pomraning and R. Sanchez, *The use of renewal theory for stochastic transport*, Journal of Quantitative Spectroscopy & Radiative Transfer **43** (1990), no. 4, 267-270.
24. B. J. Su and G. C. Pomraning, *Benchmark results for particle-transport in binary non-markovian mixtures*, Journal of Quantitative Spectroscopy & Radiative Transfer **50** (1993), no. 2, 211-226.
25. F. Malvagi, G. C. Pomraning and M. Sammartino, *Asymptotic diffusive limits for transport in markovian mixtures*, Nuclear Science and Engineering **112** (1992), no. 3, 199-214.
26. F. Malvagi and G. C. Pomraning, *Renormalized equations for linear transport in stochastic media*, Journal of Mathematical Physics **31** (1990), no. 4, 892-900.
27. G. C. Pomraning, *A stochastic eigenvalue problem*, Annals of Nuclear Energy **26** (1999), no. 3, 217-235.
28. M. M. R. Williams and E. W. Larsen, *Neutron transport in spatially random media: Eigenvalue problems*, Nuclear Science and Engineering **139** (2001), no. 1, 66-77.
29. S. Miller, *A stochastic method for brownian-like optical transport calculations in anisotropic biosuspensions and blood*, Journal of Mathematical Physics **39** (1998), no. 3, 1534-1550.
30. G. C. Pomraning, *Diffusive transport in binary anisotropic stochastic mixtures*, Annals of Nuclear Energy **19** (1992), no. 10-12, 737-763.

31. M. M. Selim, M. S. A. Krim, M. T. Attia and S. A. El Wakil, *Stochastic radiative transfer in a finite plane with anisotropic scattering in a binary markovian mixture*, Waves in Random Media **9** (1999), no. 3, 327-340.
32. G. C. Pomraning, *A model for interface intensities in stochastic particle-transport*, Journal of Quantitative Spectroscopy & Radiative Transfer **46** (1991), no. 4, 221-236.
33. B. J. Su and G. C. Pomraning, *Limiting correlation length solutions in stochastic radiative-transfer*, Journal of Quantitative Spectroscopy & Radiative Transfer **51** (1994), no. 6, 893-912.
34. *Modification to a previous higher-order model for particle-transport in binary stochastic media*, Journal of Quantitative Spectroscopy & Radiative Transfer **54** (1995), no. 5, 779-801.